Linda Martina Maier, MSc

Atmospheric Rivers in Africa observed with Satellite and Reanalysis Data

Master's Thesis

Submitted in fulfillment of the requirements for the academic degree

"Master of Science - MSc"

Master's degree program in Space Sciences and Earth from Space

Submitted to

Graz University of Technology

Faculty of Electrical Engineering and Information Technology

Supervisors:

Assoz. Prof. Mag. Dr.rer.nat., Ulrich Foelsche

Bahareh Rahimi, MSc

Institute of Physics, University of Graz

Graz, December 2024

ACKNOWLEDGEMENT

I want to take a moment to thank everyone who has been there for me and supported me while I worked on this Master’s thesis.

First, I want to give a huge thank you to my supervisors, Assoc. Prof. Mag. Dr. rer. nat. Ulrich Foelsche and Bahareh Rahimi for their advice, support, and encouragement throughout this process. Their insightful feedback and guidance kept me focused and motivated, and their dedication to my success has made a lasting impact.

I am also incredibly grateful to my parents. Their love, encouragement, and belief in me have been the backbone of my academic journey. They have been there for me every step of the way, giving me the strength and reassurance during challenging times.

To my sister and brother, thank you for always listening to me, cheering me on, and making me laugh when I needed it the most. Your advice and support have been priceless, and I am so lucky to have you both by my side.

To my amazing flatmates, thank you for being my constant support system throughout this journey. Your patience in listening to my worries, offering thoughtful advice, and giving me the hugs and encouragement I needed have meant so much to me. Living with you has been a source of comfort and joy, and I truly could not have done this without your kindness and understanding.

A special thank you goes to my partner for being so understanding and patient during this journey. Your kindness and encouragement made such a difference and helped me keep going when things felt overwhelming.

From the bottom of my heart, thank you all. I truly could not have done this without you.

DECLARATION OF ORIGINALITY

I confirm that the submitted thesis is original work and was written by me without further assistance. Appropriate credit has been given where reference has been made to the work of others. The thesis was not examined before, nor has it been published. The submitted electronic version of the thesis matches the printed version.

Date: 09.12.2024 Signature: Maier L.

[Linda Martina Maier]

EXECUTIVE SUMMARY

Atmospheric Rivers (ARs) - schmale, feuchtigkeitsreiche Bänder in der Atmosphäre, die auch Atmosphärische Flüsse genannt werden - sind zentrale Elemente des globalen Wassertransports. Bislang sind diese in Afrika wenig erforscht. Diese Arbeit untersucht die Dynamik der ARs über Afrika im Zeitraum von 2009 bis 2019. Dabei wird (1) eine statistische Analyse auf kontinentaler Ebene zur Erfassung von AR-Mustern sowie (2) eine Bewertung der Genauigkeit der ERA5-Reanalysedaten im Vergleich zu Globalem Navigation Satelliten System Radio-Okkultation-Daten (GNSS RO) anhand von ausgewählten Beispielen gezeigt. Mithilfe von ERA5, CDAAC RO und der bildverarbeitungs-basierten Methode zum Tracken der atmosphärischen Flüsse (IPART) zeigt diese Studie saisonale, regionale und interannuale Variabilitäten von AR-Vorkommen in Afrika auf.

Die statistische Analyse (1) zeigt klare saisonale Trends: In Südafrika erreicht die AR-Aktivität während des süd-hemisphärischen Sommers ihren Höhepunkt. In Nordafrika treten ARs hingegen bevorzugt im borealen Winter und Frühling auf. Die vergleichende Auswertung (2) zeigt, dass ERA5 höhere Werte für die integrierte Wasserdampfsäule (IWV) angibt, während GNSS RO systematisch trockenere Werte liefert, da Wasserdampf in den unteren Atmosphärenschichten unterrepräsentiert wird. Im Einklang mit früheren Studien spiegeln diese Unterschiede die Beiträge beider Datensätze wider. Dennoch erfasst ERA5 groß-skalige IWV-Muster effektiv, was seine Nutzung für die AR-Analyse in Afrika unterstützt. Diese Forschung legt die Grundlage für zukünftige Studien zur Dynamik von ARs in Afrika und bietet wichtige Implikationen für das Wassermanagement und die Planung von Klima Resilienz.

Schlagwörter: Atmosphärische Flüsse, Afrika, ERA5-Reanalyse, GNSS-Radio-Okkultation, IPART, ARtracks, Integrierter Wasserdampf (IWV)

ABSTRACT

Atmospheric Rivers (ARs) - narrow, moisture-rich bands in the atmosphere - play a vital role in global water transport but remain understudied in Africa. This thesis explores AR dynamics across Africa from 2009 to 2019 through (1) a continent-wide statistical analysis of AR patterns and (2) an evaluation of the accuracy of ERA5 Reanalysis data compared to Global Navigation Satellite System Radio Occultation (GNSS RO) observations for selected events. Using ERA5, RO and the Image-Processing-based Atmospheric River Tracking (IPART) method, this study reveals seasonal, regional, and interannual variability in AR occurrences over Africa.

The statistical analysis (1) reveals distinct seasonal trends: Southern Africa experiences peak AR activity during the austral summer, while Northern Africa peaks in boreal winter and spring, influenced by mid-latitude weather systems. The comparative evaluation (2) shows that ERA5 indicates higher IWV values, while RO retrievals are systematically drier due to underrepresentation of low-level water vapor. Consistent with previous studies, these discrepancies reflect contributions from both datasets. Despite this, ERA5 effectively captures large-scale IWV patterns supporting its use for AR analysis in Africa. This research lays the groundwork for future studies on AR dynamics in Africa, with broader implications for water resource management and climate resilience planning.

Key words: Atmospheric Rivers, Africa, ERA5 Reanalysis, GNSS Radio Occultation, IPART, ARtracks, Integrated Water Vapor (IWV)

TABLE OF CONTENT

1. INTRODUCTION

This Master's thesis consists of two parts. The introduction outlines characteristics and importance of Atmospheric Rivers (ARs) in the global water cycle as well as details about the datasets used in this research. The second part presents a scientific paper, submitted to the *Remote Sensing* journal (MDPI) in December 2024, which focuses on the analysis of ARs over Africa.

Over 90% of water vapor moving north or south across the midlatitudes travels through narrow pathways known as Atmospheric Rivers (ARs). They are organised in elongated, narrow corridors of concentrated water vapor and play a critical role in transporting moisture across great distances. Three to five events are typically present at any time in each hemisphere. The ARs are spanning over a length of 2,000 km and a width of under 500 km (Zhu & Newell, 1994), (Chakraborty et al., 2022). ARs are characterized by their high Integrated Water Vapor (IWV) or Integrated Vapor Transport (IVT) with treshold above 2 cm or 250 kg m^{-1} s^{-1} respectively (Bozkurt et al., 2018). In addition, ARs are associated with strong winds near Earth´s surface (Gimeno et al., 2014). Comparable in flow to the Mississippi River, ARs often drive heavy rainfall and flooding, impacting water resources and extreme weather, particularly in mid-latitudes and subtropics (Gimeno et al., 2014). They are known to influence global weather patterns, particularly in regions with complex topography and dynamic climate systems (Dacre et al., 2015). To get a better understanding what an AR is, Figure 1 A shows the IWV values for an exemplary event over the northern Atlantic in 2019, while a general global AR distribution is shown in Figure 1 B.

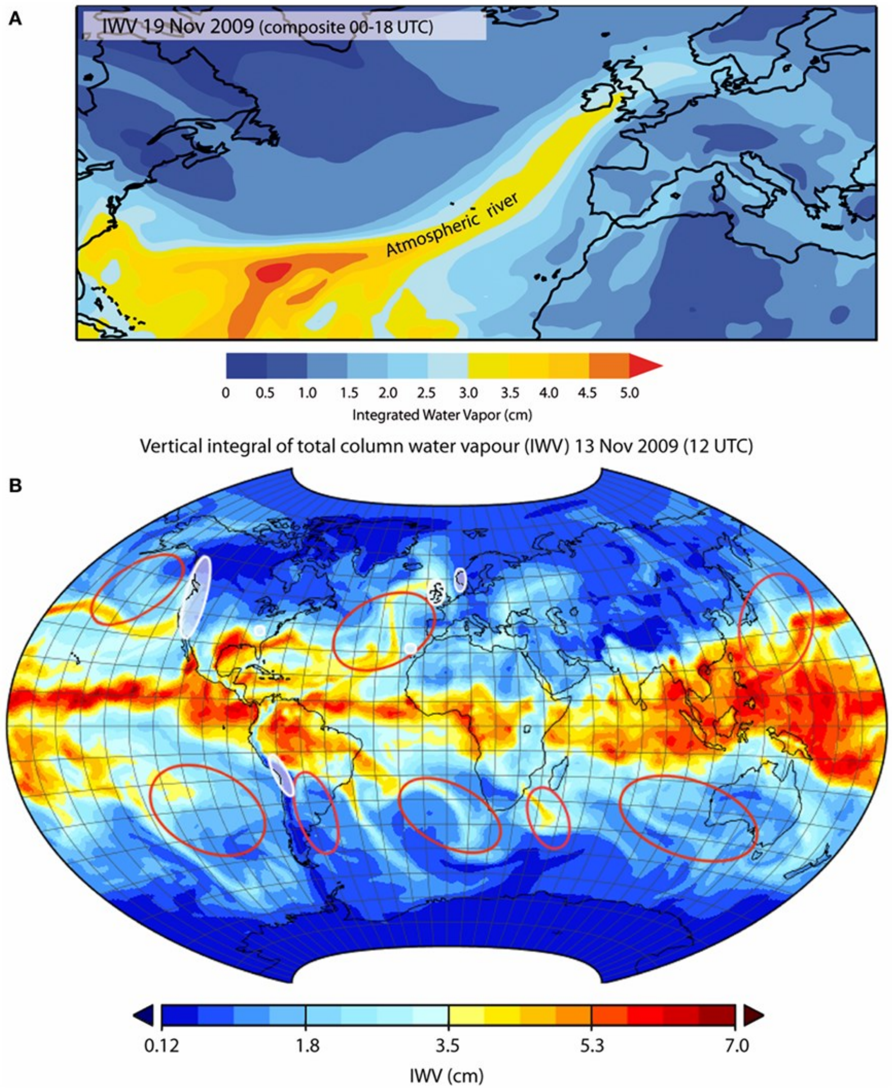

Figure 1. (A) An AR shown via Integrated Water Vapor (IWV, in cm) over the northern Atlantic on November 19, 2009. (B) Regions of typical AR occurrence (red contours) from Waliser et al. (2012) and Zhu & Newell (1998), with white contours marking areas of AR-related extreme precipitation and flooding (Gimeno et al., 2014, p.2).

The occurrence of ARs over Africa is influenced by several factors. For an AR to develop a source of atmospheric moisture is essential. The source is typically a large water body where evaporation takes place. The presence of large-scale atmospheric pressure systems, like cyclones and anticyclones, is fundamental to organizing and transporting this moisture into narrow corridors of concentrated vapor (Salimi et al., 2020).

Wind shear helps maintaining the narrow, elongated structure of the AR characteristic of ARs. Jet streams are commonly responsible for generating this wind shear, while also enabling the rapid transport of moisture (Gimeno et al., 2016). ARs are most frequently observed over oceans and mid-latitude regions, with strong activity along the west coasts of continents. Key regions include North America, Europe's Atlantic coast, the Andes, Japan, and parts of Africa. Southern Hemisphere ARs are less studied, but activity occurs near Australia, New Zealand, and Antarctica. AR frequency typically decreases toward the poles, with the highest concentrations over oceanic areas (Guan & Waliser, 2019).

ARs are often associated with cyclones or weather fronts, where rising air over mountains or colder air masses causes the water vapor to condense, leading to heavy rain or snow (Gimeno et al., 2014). Their ability to transport large volumes of water vapor from oceanic sources to inland areas makes them essential in driving both beneficial rainfall and hazardous flooding (Dacre et al., 2015). Due to their hydrological impact ARs have mainly been studied in Northern Africa and Europe. In the western United States, play a significant role in delivering a large share of the annual precipitation, particularly in California. For instance, research by Gershunov et al. (2017) indicates that ARs can account up to 50% of the state´s total rainfall in, replenishing water resources while also posing flood risks. In Europe, ARs have been linked to extreme rainfall and flooding in regions such as the United Kingdom and the Iberian Peninsula. Lavers and Villarini, (2013) demonstrated that ARs are responsible for approximately 80% of extreme precipitation events in the UK. On a global scale, ARs contribute roughly 30% of total precipitation, playing a crucial role in delivering moisture to arid and semi-arid regions, sustaining ecosystems, and supporting freshwater resources through their impact on snowpack accumulation in mountainous areas. The heavy rainfall, however, can lead to flooding, landslides, soil erosion and debris flow. Additionally, the high winds accompanying ARs can trigger avalanches and impact forest ecosystems (Dettinger et al., 2011), (Wang et al., 2023).

ARs can be distinguished from tropical cyclones or monsoons by their typical narrow and long shape and their short appearance which lasts from a few hours to several days. Additionally, ARs are characterised by their horizontal moisture transport along the "river in the sky," while monsoons mainly involve vertical moisture movement (Gimeno et al., 2016).

Given their role in extreme weather, recognizing AR dynamics has implications for water resource management, climate forecasting, and disaster preparedness worldwide. This study applies these global insights to the African continent, where the pathways and impacts of ARs remain less understood. While ARs are increasingly recognized for their role in shaping global weather patterns, their behaviour over Africa remains poorly understood. Previous research has primarily focused on AR dynamics in North America and Europe, with limited emphasis on the African continent. Addressing this gap, we apply advanced tracking methods like IPART and high-resolution datasets, such as GNSS RO and ERA5, to analyse AR activity. By exploring their seasonal trends and validating data accuracy, we want to provide actionable insights for water resource management and climate resilience in Africa.

1.1. ATMOSPHERIC RIVERS OVER AFRICA

ARs have dual impacts: they provide critical freshwater resources to regions like the Western Cape, but they also pose risks such as flooding and infrastructure damage during extreme events. For example, a 2010 AR event caused widespread flooding in Morocco, impacting urban centres like Casablanca (Akbary et al., 2019). Climate projections suggest potential increases in AR intensity due to warming oceans, underscoring the need for focused research (Wang et al., 2023). In Southern Africa, especially the Western Cape, ARs account for up to 70% of extreme winter rainfall days (Blamey et al., 2018). Although ARs are less frequent in Africa compared to regions like North America, they play a crucial role in delivering precipitation to arid and semi-arid areas. Their impacts are more prominent along coastal areas, where moisture transport interacts with orographic features to enhance precipitation. The understanding of their temporal and spatial variability remains limited. Recent studies, however, have expanded our understanding of ARs in Africa. For instance, research has identified "aerosol atmospheric rivers" (AARs), which transport aerosols like dust and smoke within an AR (Chakraborty et al., 2021), (Rautela et al., 2024).

1.1.1. Moisture Origins and Atmospheric Dynamics of ARs in Africa

In Africa, ARs shape regional weather patterns and rainfall. Latest research indicates moisture sources including the Atlantic Ocean, Arabian Sea, and Red Sea (Akbary et al., 2019), (Esfandiari & Shakiba, 2024). The North Atlantic Ocean holds significant importance in the transport of water vapor eastward toward Africa, shaping rainfall patterns in areas such as Northern Africa and the Middle East. In contrast, ARs affecting Southern Africa usually source moisture from the South Atlantic Ocean and tropical regions, where they interact with extratropical cyclones and cold fronts, resulting in intense rainfall events (Ramos et al., 2019).

Northern Africa

The primary sources of moisture for ARs over Africa include the Arabian Sea, the Red Sea, and the Atlantic Ocean, with the North Atlantic serving as a key contributor to ARs impacting Northern Africa and the Middle East. The Red Sea acts as a significant convergence zone where moist air from multiple directions converges and rises due to the influence of local topography (Akbary et al., 2019).

Moisture transport is significantly influenced by the interplay between upper-level cyclonic systems and anticyclonic circulations within the lower to middle troposphere. For example, an anticyclonic system over the Arabian Sea can amplify the northward movement of moisture originating from the Gulf of Aden and the southern Red Sea. Additionally, the position and configuration of jet streams significantly affect AR development (Esfandiari & Shakiba, 2024). In Africa, the subtropical jet stream often merges with the polar jet stream, creating a more meridional circulation pattern that supports vapor transport. This merger facilitates the rapid movement and concentration of moisture, contributing to AR formation. Furthermore, mountain ranges, like the western topography of the Red Sea, play a role in the ascent and concentration of saturated air (Esfandiari & Shakiba, 2024).

Influence of the North Atlantic and NAO

In Northern Africa, the behaviour of ARs is closely tied to the North Atlantic Oscillation (NAO), a climate pattern characterized by fluctuations in atmospheric pressure between the Icelandic Low and the Azores High (Hurrell et al., 2003). During the positive phase of the NAO, a strengthened pressure gradient strengthens the westerlies, allowing ARs to extend further into Northern Africa. As ARs move eastward from their origin over the North Atlantic, they often make landfall in Mauritania and Senegal, continuing across North Africa and into the Middle East, influencing rainfall in Saudi Arabia and beyond. The subtropical jet stream, which merges with the polar jet stream, is crucial in guiding these ARs, enhancing their moisture transport and intensity (Akbary et al., 2019). The Red Sea acts as an "atmospheric well," providing additional moisture and intensifying AR-related precipitation as these systems move across Egypt and into the Middle East (Esfandiari & Shakiba, 2024).

Southern Africa

Weather patterns associated with ARs in Southern Africa typically involve the transport of moist air from the South Atlantic Ocean, and in some cases, from as far as South America.

These ARs carry water vapor from tropical and subtropical regions in the Southern Hemisphere, which precipitates as heavy rainfall when the ARs interact with the mountainous terrain of the Western Cape. This orographic effect enhances rainfall, contributing to local watersheds and reservoirs (Blamey et al., 2018), (Ramos et al., 2018), (Gimeno-Sotelo & Gimeno, 2022).

Research by Ramos et al. (2018) using Lagrangian analysis identified the South Atlantic Ocean and parts of South America as key moisture sources for ARs reaching South Africa. During AR events, moisture is transported from these regions towards the Western Cape. The study highlighted the role of the South American Low-Level Jet (SALLJ), particularly during phases such as the no Chaco jet event (NCJE), in transporting moisture from the Amazon basin towards the South Atlantic, which then feeds into the ARs impacting South Africa. The sources of moisture affecting the Western Cape can be traced to four main regions. Firstly, the western South Atlantic Ocean, between 20°S and 30°S, sees moisture uptake from tropical and subtropical areas. This region includes a hot spot off the central coast of Brazil, where moisture uptake intensifies during AR days due to convergence along cold fronts and extratropical cyclones moving eastward towards South Africa (Ramos et al., 2018). Secondly, a major source of moisture uptake takes place in the eastern South Atlantic Ocean, close to the Western Cape. This region, covering the Agulhas Current retroflection, directs moisture towards the area. The Agulhas Current retroflection is where the Agulhas Current, a warm current along Africa’s east coast, loops back into the Indian Ocean near South Africa's southern tip. Thirdly, the Agulhas Current, flowing along the east coast provides a stream of moisture. Lastly, land areas to the north of the Western Cape, including northern and northwestern South Africa, Namibia, and Botswana, serve as continental sources of moisture. (Ramos et al., 2018)

Interaction with SAHS and Cyclonic Systems

In Southern Africa, ARs follow a pathway, shaped by the South Atlantic Subtropical High (SASH) and the interaction with extratropical cyclones and cold fronts. The ARs typically follow a southwest to northeast trajectory, drawing moisture from the South Atlantic Ocean and sometimes as far as South America. During austral winter (JJA), ARs are more frequent, particularly during the early winter and late spring months according to Blamey et al. (2018). The Cape Fold Mountains of the Western Cape and other topographical features in the region enhance orographic rainfall. Moisture transport in this region is further influenced by the

South American Low-Level Jet (SALLJ), which can occasionally channel moisture from the Amazon Basin across the Atlantic into Southern Africa during certain phases of the NCJE (Grimm & Reason, 2015). The latitudinal positioning of ARs in Southern Africa is shifted by the strength and position of the SASH, determining how far inland ARs can penetrate.

1.1.2. Seasonal and Interannual Variability

ARs over Africa are subject to seasonal and interannual variability, driven by the interactions between global climate oscillations and regional weather patterns, as described before. In Northern Africa, AR activity peaks during the boreal fall and winter, when the Azores High retreats, allowing more moisture-laden air to penetrate the region (Akbary et al., 2019). Conversely, during the boreal summer, AR activity decreases due to the dominance of the Azores High and stable atmospheric conditions.

In Southern Africa, AR activity is highly seasonal, peaking during the austral winter (Blamey et al., 2018). The year-to-year variability of the events is further modulated by large-scale climate patterns, including El Niño-Southern Oscillation (ENSO) and the Southern Annular Mode (SAM), which affect both the frequency and intensity of ARs across the continent (Reason, 2001).

1.2. Societal Relevance

ARs hold significant societal relevance due to their role in shaping precipitation patterns, supporting water resources, and causing extreme weather events. Scientists emphasize that understanding of climate and atmospheric patterns can have transformative impacts on public health, agricultural productivity, and overall resilience.

Dezfuli et al. (2021) studies the contribution of ARs to major flood events in the Middle East, where ARs not only affects water resources but also enables dust transport across arid regions. This impacts air quality and health in downwind areas. De Longueville et al. (2010) addresses the health implications of desert dust exposure in West Africa, emphasizing the urgent need for localized research to fight respiratory and other health conditions caused by pollutants. Furthermore, Thandlam et al. (2022) points to the ARs influence on precipitation extremes. This is essential in understanding flood risks and planning for climate resilience in vulnerable regions. In a broader African context, Papa et al. (2023) underscores their critical role in regional water resource variability. Especially as satellite monitoring enables better forecasting and management of hydrological resources. This is important for the growing population and agricultural needs. Vaughan et al. (2019) further stress the need for investment IN weather and climate service infrastructure. Conway (2011) argues that in sub-Saharan Africa, where communities depend on small-scale agriculture, linking climate science with development activities is essential for enhancing adaptive capacity. This is especially important because climate change is increasing the frequency and intensity of extreme weather events.

Together, these studies underscore the societal benefits of advancing AR research, which supports more effective health interventions, sustainable agricultural practices, and the resilience of infrastructure in the face of climate challenges (Conway, 2011), (De Longueville et al., 2010), (Dezfuli et al., 2021), (Thandlam et al., 2022), (Baki et al., 2023), (Papa et al., 2023).

1.3. RESEARCH GAP AND OBJECTIVE

The primary objective of this thesis is to address the knowledge gaps in AR behaviour over Africa by analysing their seasonal, regional, and interannual variability from 2009 to 2019. Unlike conventional AR studies, which often rely solely on reanalysis datasets, this work validates ERA5's IWV estimates against GNSS RO data. Specifically, we aim to evaluate the accuracy of ERA5 IWV data to offer insights for high-moisture conditions. By applying IPART, we seek to identify AR landfall patterns and improve the understanding of AR dynamics over the whole continent. The application of IPART allows for precise AR tracking based on spatiotemporal characteristics, independent of magnitude thresholds.

This work thus provides a framework for identifying ARs in Africa, enabling more precise studies of their role in the continent's hydrological and climatic systems. It bridges knowledge gaps by introducing high-resolution datasets offering a baseline for exploring AR contributions to rainfall variability and extreme events. The validation of ERA5 with GNSS RO data contributes to improving reanalysis datasets, which are crucial for climate modeling and risk assessment globally.

2. DATA

This chapter aims to give a more in-depth understanding of the data used. While the paper written in the framework of this thesis already includes information, this section complements the information by providing more detailed exploration on the datasets.

Data sources used to analyse AR events, include ERA5 Reanalysis data, GNSS RO data and IPART. ERA5 provides high-resolution historical climate data essential for tracking hourly water vapor profiles, while RO data offers vertical profiles of atmospheric moisture and IPART, an image-processing-based method, enables precise tracking over land. The ARtracks catalogue, based on ERA5 and IPART, is used to identify AR landfall locations, supporting the study of AR impacts on targeted regions.

The chosen study period, 2009–2019, provides an ideal period for analysing AR dynamics over Africa. This decade allows for a robust examination of seasonal, regional, and interannual variability while aligning with the availability of high-resolution datasets, such as ERA5 Reanalysis data and RO data. For this period high quality data and spatial-temporal resolution, which enhance the accuracy of tracking and analysing AR patterns, are available. The selection of this period therefore balances data reliability with the ability to capture meaningful trends, offering a solid foundation for understanding AR contributions to Africa's hydrological cycle.

2.1.1. ERA5 Reanalysis

ERA5 Reanalysis data was used for the interpolation and comparison with RO data. We obtained data from the ERA5 hourly data on single level from 1940 to present data set available on the CDS website (Hersbach et al., 2020). The "Reanalysis" product type was chosen due to its broad historical climate data. Within the "Other" catalogue, the variable Total Column Water Vapor (TCWV) is selected. Hourly data was collected for the specific day of the landfalling AR event. The required sub-region was extracted based on the geographical area necessary for the event.

ERA5 Reanalysis data, produced by the Copernicus Climate Change Service (C3S), offers a detailed record of global climate patterns dating from 1940 onwards. The data, accessible through the Climate Data Store (CDS), is available at a 0.25° spatial resolution, with hourly, daily, and monthly temporal resolutions.

(https://www.ecmwf.int/en/forecasts/dataset/ecmwf-Reanalysis-v5, last access: 03.10.2024).

Reanalysis data is produced by combining observational data with model data to create a consistent time series of climate information. The ERA5 Reanalysis is based on the Integrated Forecast System (IFS), a numerical weather prediction model created by the ECMWF. ERA5 combines data from satellites, ground-based instruments like radiosondes and weather stations, and ship- and aircraft-based observations using the 4D-Var data assimilation technique. This approach works by reducing discrepancies between the model's output and observational data over a specified time, thereby enhancing the accuracy of the forecast and aligning the model more closely with actual observations. The IFS model simulates the atmosphere of Earth, providing a framework for integrating observational data. Quality control procedures are applied to the observational data before incorporation. This ensures the reliability and accuracy of the Reanalysis product. (Hersbach et al., 2020), (Copernicus Knowledge Base: ERA5 Data Documentation, 2024)

2.1.2. GNSS Radio Occultation Data

In this research, reprocessed Level 2 wet data (https://data.cosmic.ucar.edu/gnss-ro/, last access: 03.10.2024) from a range of satellites, specifically TerraSar-X (TXS), Gravity Recovery and Climate Experiment (GRACE), Constellation Observing System for Meteorology, Ionosphere, and Climate-1 (COSMIC-1, 6 satellites), Meteorological Operational Satellites (Metop series), PAZ and the Korean Multi-Purpose Satellite-5 (Kompsat 5) is utilized. The data is sourced from the COSMIC Data Analysis and Archive Center (CDAAC). Level 2 data represents processed information derived from raw Radio Occultation (RO) measurements, including variables such as atmospheric temperature, pressure, and humidity. This data is then post-processed to improve accuracy (University Corporation for Atmospheric Research, 2024).

GNSS RO is well-suited for examining ARs from 2009 to 2019 because of its worldwide coverage, ability to operate in all weather conditions, and vertical resolution (Shao et al., 2023). It provides consistent, accurate measurements of water vapor and temperature, capturing the structure and intensity of ARs even in severe weather. Its stability over time also makes it well-suited for long-term trend analysis, offering insights for climate research and weather modelling (S. Ho et al., 2010), (Steiner et al., 2011), (S.-P. Ho et al., 2018), (Rahimi & Foelsche, 2024). RO has its origins in the 1960s, when scientists used the Mariner

3 and 4 satellites to study the atmosphere of Mars (Fjeldbo & Eshleman, 1968). In 1995, the GPS/MET mission adapted this technique for Earth's atmosphere, proving its potential for high-resolution atmospheric profiling. Following missions like CHAMP, SAC-C, and FORMOSAT-3/COSMIC further confirmed and expanded the use of RO for weather, climate, and ionospheric studies (Fjeldbo & Eshleman, 1965).

The atmosphere can be measured with this technique by observing the changes in a radio signal as it passes through the medium. This method involves satellites in low-earth orbit (LEO) equipped with receivers that detect the bending of GNSS signals. As the radio signal passes through the atmosphere, it experiences refraction due to changes in atmospheric density, which vary with altitude, temperature, pressure, and humidity. The bending angles measured provide insights into the vertical structure of the atmosphere (Steiner et al., 2011).

The primary observable in RO is the phase delay of the GNSS signal caused by its passage through the atmosphere. By measuring this phase delay at multiple frequencies, vertical profiles of the bending angles of the radio wave trajectories are obtained (Anthes, 2011). From these bending angles, profiles of atmospheric refractivity are derived (Rahimi & Foelsche, 2024). The concept of RO is shown in Figure 2.

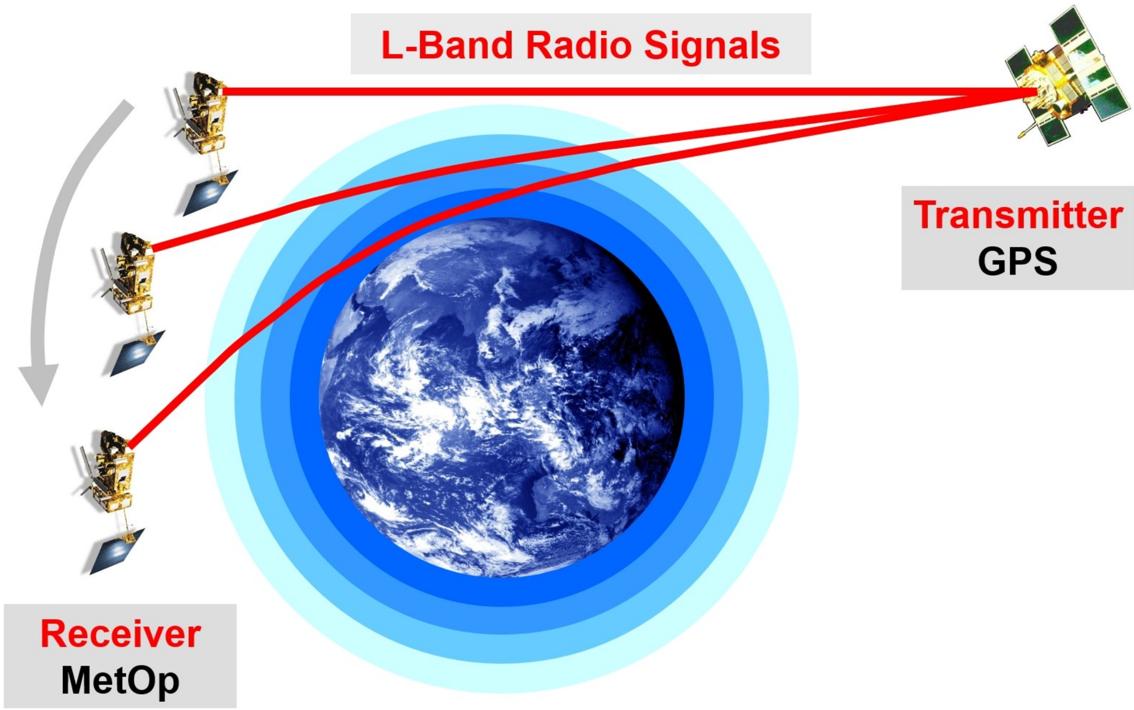

Figure 2. Radio Occultation Scheme (source: Ulrich Foelsche, pers. comm.)

Retrieving vertical profiles of water vapor involves several critical steps. Initially, as GNSS signals cross the atmosphere, they experience bending and delay due to refraction influenced by atmospheric conditions (Rahimi & Foelsche, 2024). The bending angles of these signals are measured, providing essential data on refractivity. Using these bending angles, refractivity profiles are derived through an Abel inversion. The refractivity N is a function of pressure P, temperature T, and the partial pressure of water vapor P_W, as described by Equation 1.

$$\mathrm{N} = 77.6\,\frac{P}{T} + 3.73 \times 10^5\,\frac{P_W}{T^2} \qquad (1)$$

Given the refractivity, a one-dimensional variational (1D-Var) retrieval algorithm is then used to extract temperature and water vapor profiles. This method combines RO data with background atmospheric models, such as those from the ECMWF, to enhance accuracy. This process allows for near-vertical profiles of water vapor to be retrieved. (S. Ho et al., 2010), (Ahmed et al., 2022).

Data processing in RO initially uses geometric optics to interpret the signal bending. However, this method encounters difficulties in the lower troposphere due to multipath propagation. Techniques like wave optics are employed to handle the signal complexity more effectively, providing accurate bending angles, especially in the lower atmosphere. This enables RO to achieve high vertical resolution, approximately 0.1 km near the surface and up to 1 km in the stratosphere. This makes it superior to other remote sensing methods in resolving fine atmospheric layers (Vaquero-Martínez & Antón, 2021), (Steiner et al., 2011).

2.1.3. SSMIS

The Special Sensor Microwave Imager Sounder (SSMIS) and the Special Sensor Microwave Imager Sounder (SSM/I) have been used on Defence Meteorological Satellite Program (DMSP) satellites since the late 1980s. SSMIS is an enhanced version of SSM/I, adding the ability to profile temperature in the upper atmosphere. The SSMIS collects data from 24 channels, ranging from 19 to 183 GHz. The SSMIS sources data from temperature and moisture, surface properties, and precipitation. This allows for the construction of temperature profiles of the atmosphere. The instrument measures humidity levels in different atmospheric layers. Microwave signals penetrate clouds and provide data on surface properties such as soil moisture, sea surface temperatures, and sea ice concentrations (Wentz et al., 2012). The SSMIS uses a conical scan technique, rotating around a vertical axis to scan a swath of the Earth's surface beneath the satellite. (Observing Systems Capability Analysis and Review Tool (OSCAR), 2024).

To visualise SSM/I and SSMIS data, graphic browse images are available (SSM/I and SSMIS data are produced by Remote Sensing Systems. Data are available at www.remss.com/missions/ssmi, last access: 03.12.2024). Figure 3 shows the global distribution of atmospheric water vapor given in mm with data from the F16 instrument on the 26th of September 2009. Red and pink indicate higher and purple and blue lower amounts of vapor.

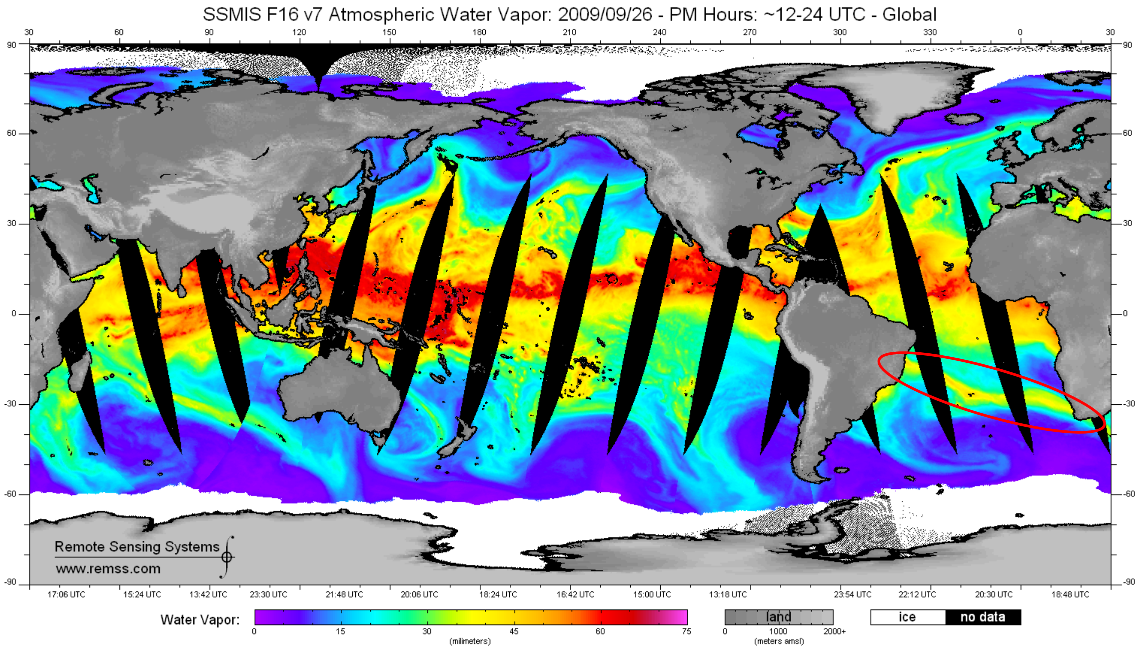

Figure 3. SSMIS Visualisation of global water vapor (mm) distribution with SSMIS data on 26.09.2009 between 12 and 24 UTC. Red contour shows South Africa 2009 event (later analysed) (Wentz et al., 2012).

For tracking ARs over land, additional techniques such as the Image-Processing based Atmospheric River Tracking (IPART) method are valuable. While SSMIS excels at capturing oceanic moisture, the complex terrain and varied surface properties over land necessitate additional methods for tracking ARs accurately.

2.1.4. IPART

To identify AR events, the Image-Processing-based Atmospheric River Tracking (IPART) is used. IPART is further utilized for the statistical analysis of ARs over Africa (https://github.com/ihesp/IPART, last access: 14.11.2024).

The IPART method, developed by Xu et al. (2020) represents an advancement in the detection and tracking of ARs (Xu et al., 2020). Traditional methods of AR detection have heavily relied on magnitude thresholding of IWV and Integrated Vapor Transport (IVT). This Method offers an approach that is independent of magnitude. It focuses on the spatiotemporal characteristics of ARs. Traditional thresholding methods assume a constant moisture level throughout the study period and rely on historical observations. One common approach involves setting IWV threshold to greater than 2 cm, as studied by Ralph et al. (2004) or Dettinger (2011), combined with conditions such as a minimum length of 2000 km and a maximum width of 1000 km. Another approach uses a minimum IVT value of 250 kg m^{-1} s^{-1}, as applied by Rutz et al. (2014). An alternative to fixed thresholds is using a specific percentile of IWV or IVT, which accounts for seasonal differences and distinguishes between midlatitude and polar systems, as demonstrated by Guan and Waliser (2017). This percentile-based method is more robust in adapting to varying climatic conditions.

At the core of the IPART method is the top-heat by reconstruction (THR) algorithm, a technique known from image processing, which is designed to detect structures in noisy data and helps emphasize the spatial continuity of AR features (Zhu & Newell, 1994). The THR algorithm involves several steps including greyscale erosion, greyscale dilation and anomalous IVT identification. The subtraction of a "greyscale reconstruction by dilation" image from the original greyscale image is the IVT distribution. The process begins with defining a "marker" image of the IVT data, using a technique called greyscale erosion. This reduces noise and highlights core regions of moisture. The next step expands the highlighted regions, which is called the greyscale dilation. When this spread-out version is overlaid with the original IVT distribution, it creates a "reconstruction" that captures the primary areas of moisture. Comparing the original IVT data with this reconstructed version highlights areas with high moisture, which could indicate potential ARs (Xu et al., 2020).

To identify the AR's central path or "axis," the method uses a new technique: it builds a topological graph based on AR region coordinates and the direction of moisture flow. Finding the AR axis then becomes a matter of searching for the best path within this graph. This approach ensures that the identified axis accurately follows the main direction of moisture flow, staying within the AR boundary and providing a realistic representation of the AR's location and extent. This axis serves as a simple curve that shows the AR's path across a region, summarizing its overall orientation and reach (Xu et al., 2020).

2.1.4.1. ARtracks

The *"[...] Global Atmospheric River Catalogue Based on ERA5 and IPART [...]"*, known as ARtracks is used to find the landfall location of the AR events studied (https://github.com/dominiktraxl/artracks, last access: 14.11.2024) (Traxl, 2022). It provides a global AR catalogue based on the ERA5 Reanalysis dataset and IPART, allowing to detect, analyze and visualize events. The repository provides a tool for studying the AR axis, or path, over time, and the location of the landfall. The calculation of the landfall location is based on meteorological data, like IVT (Traxl, 2022).

In our study we utilized ARtracks to study AR events from 2009 to 2019. Specifically, we identified an increase in the event axis as it moved towards the African continent. We focused on events whose longitudes and latitudes fell within the geographical boundaries of Africa, which was achieved by using coordinates to create a polygon that closely approximates the shape of the African continent. The Shapely library, a Python package for manipulation and analysis of planar geometric objects, was employed to construct these boundaries. Additionally, Cartopy, a library designed for geospatial data processing, was used to check if each AR's landfall location fell within the defined boundaries of Africa. This initial screening was crucial in narrowing down the number of events to those potentially impacting the continent. The identified axis was later used to show the path of the AR for the studied events.

2.2. CHALLENGES AND LIMITATIONS

The initial methodology aimed to integrate Special Sensor Microwave Imager Sounder (SSMIS) data with ERA5 Reanalysis data to improve the temporal and spatial resolution of atmospheric analysis. Particularly for studying IWV and temperature profiles in the context of the chosen AR events. SSMIS, operating a series of instruments (e.g., F16, F17), provides valuable microwave measurements that capture atmospheric variables. However, integrating SSMIS with ERA5 and RO proved challenging due to temporal and spatial constraints. The satellite has a 12-hour orbit pattern, providing two maps of atmospheric conditions per location each day. This temporal resolution limits the number of instances available for comparison. Thus, it is insufficient for tracking fast-evolving weather phenomena,

Moreover, effective interpolation between SSMIS and RO data requires at least 20 events within narrow, precisely timed windows to ensure robust statistical alignment. This condition was rarely met, as RO data within the required windows was too sparse. Various approaches were considered, including relaxing temporal constraints (e.g., allowing data matches within a ±2 or 3-hour range) or focusing solely on spatial resolution while ignoring exact timing, but both options introduced considerable trade-offs. Relaxing time requirements compromised temporal accuracy, while focusing only on spatial resolution limited the ability to capture accurate atmospheric dynamics over time. Further complicating the integration, the RO data had isolated event counts for certain atmospheric conditions, particularly during SSMIS overpasses.

Due to these technical limitations and time constraints, a complete integration of SSMIS data into the ERA5-based analysis was considered not viable. This decision reflects the need for alternative approaches or more adaptable datasets for capturing high-resolution atmospheric insights in future research.

The primary obstacles stem from temporal misalignment, sparse RO data within the necessary windows, and interpolation constraints. Current solutions provide partial improvements but lack precision. An alternative approach may involve loosening time-matching criteria while simultaneously exploring methods to make the spatial analysis more robust. Additionally, further exploration of both high data density with lower temporal resolution and precise time-matched profiles could offer insights into which method yields the best results for specific applications.

LIST OF REFERENCES

Ahmed, I. F., El-Fatah, M. A. A., Mousa, A. E.-K., & El-Fiky, G. (2022). Analysis of the differences between GPS radio occultation and radiosonde atmosphere profiles in Egypt. *The Egyptian Journal of Remote Sensing and Space Science*, *25*(2), 491–500. https://doi.org/https://doi.org/10.1016/j.ejrs.2022.02.006

Akbary, M., Salimi, S., Hosseini, S. A., & Hosseini, M. (2019). Spatio-temporal changes of atmospheric rivers in the Middle East and North Africa region. *International Journal of Climatology*, *39*(10), 3976–3986. https://doi.org/https://doi.org/10.1002/joc.6052

Anthes, R. A. (2011). Exploring Earth’s atmosphere with radio occultation: contributions to weather, climate and space weather. *Atmospheric Measurement Techniques*, *4*(6), 1077–1103. https://doi.org/10.5194/amt-4-1077-2011

Baki, P., Rabiu, B., Amory-Mazaudier, C., Fleury, R., Cilliers, P. J., Adechinan, J., Emran, A., Bounhir, A., Cesaroni, C., Dinga, J. B., Doherty, P., Gaye, I., Ghalila, H., Grodji, F., Habarulema, J.-B., Kahindo, B., Mahrous, A., Messanga, H., Mungufeni, P., … Zerbo, J.-L. (2023). The Status of Space Weather Infrastructure and Research in Africa. *Atmosphere*, *14*(12). https://doi.org/10.3390/atmos14121791

Blamey, R. C., Ramos, A. M., Trigo, R. M., Tomé, R., & Reason, C. J. C. (2018). The Influence of Atmospheric Rivers over the South Atlantic on Winter Rainfall in South Africa. *Journal of Hydrometeorology*, *19*(1), 127–142. https://doi.org/10.1175/JHM-D-17-0111.1

Bozkurt, D., Rondanelli, R., Marín, J. C., & Garreaud, R. (2018). Foehn Event Triggered by an Atmospheric River Underlies Record-Setting Temperature Along Continental Antarctica. *Journal of Geophysical Research: Atmospheres*, *123*(8), 3871–3892. https://doi.org/https://doi.org/10.1002/2017JD027796

Chakraborty, S., Guan, B., Waliser, D. E., & da Silva, A. M. (2022). Aerosol atmospheric rivers: climatology, event characteristics, and detection algorithm sensitivities. *Atmospheric Chemistry and Physics*, *22*(12), 8175–8195. https://doi.org/10.5194/acp-22-8175-2022

Chakraborty, S., Guan, B., Waliser, D. E., da Silva, A. M., Uluatam, S., & Hess, P. (2021). Extending the Atmospheric River Concept to Aerosols: Climate and Air Quality

Impacts. *Geophysical Research Letters*, *48*(9), e2020GL091827. https://doi.org/https://doi.org/10.1029/2020GL091827

Conway, D. (2011). Adapting climate research for development in Africa. *WIREs Climate Change*, *2*(3), 428–450. https://doi.org/https://doi.org/10.1002/wcc.115

Copernicus Knowledge Base: ERA5 data documentation. (2024).

Dacre, H. F., Clark, P. A., Martinez-Alvarado, O., Stringer, M. A., & Lavers, D. A. (2015). How Do Atmospheric Rivers Form? *Bulletin of the American Meteorological Society*, *96*(8), 1243–1255. https://doi.org/10.1175/BAMS-D-14-00031.1

De Longueville, F., Hountondji, Y.-C., Henry, S., & Ozer, P. (2010). What do we know about effects of desert dust on air quality and human health in West Africa compared to other regions? *Science of The Total Environment*, *409*(1), 1–8. https://doi.org/https://doi.org/10.1016/j.scitotenv.2010.09.025

Dettinger, M. D., Ralph, F. M., Das, T., Neiman, P. J., & Cayan, D. R. (2011). Atmospheric Rivers, Floods and the Water Resources of California. *Water*, *3*(2), 445–478. https://doi.org/10.3390/w3020445

Dezfuli, A., Bosilovich, M. G., & Barahona, D. (2021). A Dusty Atmospheric River Brings Floods to the Middle East. *Geophysical Research Letters*, *48*(23), e2021GL095441. https://doi.org/https://doi.org/10.1029/2021GL095441

Esfandiari, N., & Shakiba, A. (2024). The extraordinary atmospheric rivers analysis over the Middle East: Large-scale drivers, structure, effective sources, and precipitation characterization. *Dynamics of Atmospheres and Oceans*, *105*, 101430. https://doi.org/https://doi.org/10.1016/j.dynatmoce.2023.101430

Fjeldbo, G., & Eshleman, V. R. (1965). The bistatic radar-occultation method for the study of planetary atmospheres. *Journal of Geophysical Research (1896-1977)*, *70*(13), 3217–3225. https://doi.org/https://doi.org/10.1029/JZ070i013p03217

Fjeldbo, G., & Eshleman, V. R. (1968). The atmosphere of mars analyzed by integral inversion of the Mariner IV occultation data. *Planetary and Space Science*, *16*(8), 1035–1059. https://doi.org/https://doi.org/10.1016/0032-0633(68)90020-2

Gershunov, A., Shulgina, T., Ralph, F. M., Lavers, D. A., & Rutz, J. J. (2017). Assessing the climate-scale variability of atmospheric rivers affecting western North America.

Geophysical Research Letters, *44*(15), 7900–7908. https://doi.org/https://doi.org/10.1002/2017GL074175

Gimeno, L., Dominguez, F., Nieto, R., Trigo, R., Drumond, A., Reason, C. J. C., Taschetto, A. S., Ramos, A. M., Kumar, R., & Marengo, J. (2016). Major Mechanisms of Atmospheric Moisture Transport and Their Role in Extreme Precipitation Events. *Annual Review of Environment and Resources*, *41*(Volume 41, 2016), 117–141. https://doi.org/https://doi.org/10.1146/annurev-environ-110615-085558

Gimeno, L., Nieto, R., Vázquez, M., & Lavers, D. (2014). Atmospheric rivers: a mini-review. *Frontiers in Earth Science*, *2*. https://doi.org/10.3389/feart.2014.00002

Gimeno-Sotelo, L., & Gimeno, L. (2022). Concurrent extreme events of atmospheric moisture transport and continental precipitation: The role of landfalling atmospheric rivers. *Atmospheric Research*, *278*, 106356. https://doi.org/https://doi.org/10.1016/j.atmosres.2022.106356

Grimm, A., & Reason, C. (2015). Intraseasonal Teleconnections between South America and South Africa. *Journal of Climate*, *28*, 151016095356006. https://doi.org/10.1175/JCLI-D-15-0116.1

Guan, B., & Waliser, D. E. (2017). Atmospheric rivers in 20 year weather and climate simulations: A multimodel, global evaluation. *Journal of Geophysical Research: Atmospheres*, *122*(11), 5556–5581. https://doi.org/https://doi.org/10.1002/2016JD026174

Guan, B., & Waliser, D. E. (2019). Tracking Atmospheric Rivers Globally: Spatial Distributions and Temporal Evolution of Life Cycle Characteristics. *Journal of Geophysical Research: Atmospheres*, *124*(23), 12523–12552. https://doi.org/https://doi.org/10.1029/2019JD031205

Hersbach, H., Bell, B., Berrisford, P., Hirahara, S., Horányi, A., Muñoz-Sabater, J., Nicolas, J., Peubey, C., Radu, R., Schepers, D., Simmons, A., Soci, C., Abdalla, S., Abellan, X., Balsamo, G., Bechtold, P., Biavati, G., Bidlot, J., Bonavita, M., … Thépaut, J.-N. (2020). The ERA5 global reanalysis. *Quarterly Journal of the Royal Meteorological Society*, *146*(730), 1999–2049. https://doi.org/https://doi.org/10.1002/qj.3803

Ho, S., Zhou, X., Kuo, Y.-H., Hunt, D., & Wang, J. (2010). Global Evaluation of Radiosonde Water Vapor Systematic Biases using GPS Radio Occultation from COSMIC and

ECMWF Analysis. *Remote Sensing*, *2*(5), 1320–1330. https://doi.org/10.3390/rs2051320

Ho, S.-P., Peng, L., Mears, C., & Anthes, R. A. (2018). Comparison of global observations and trends of total precipitable water derived from microwave radiometers and COSMIC radio occultation from 2006 to 2013. *Atmospheric Chemistry and Physics*, *18*(1), 259–274. https://doi.org/10.5194/acp-18-259-2018

Hurrell, J. W., Kushnir, Y., Ottersen, G., & Visbeck, M. (2003). An Overview of the North Atlantic Oscillation. In *The North Atlantic Oscillation: Climatic Significance and Environmental Impact* (pp. 1–35). American Geophysical Union (AGU). https://doi.org/https://doi.org/10.1029/134GM01

Lavers, D. A., & Villarini, G. (2013). The nexus between atmospheric rivers and extreme precipitation across Europe. *Geophysical Research Letters*, *40*(12), 3259–3264. https://doi.org/https://doi.org/10.1002/grl.50636

Observing Systems Capability Analysis and Review Tool (OSCAR). (2024). *Instrument SSMIS*.

Papa, F., Crétaux, J.-F., Grippa, M., Robert, E., Trigg, M., Tshimanga, R. M., Kitambo, B., Paris, A., Carr, A., Fleischmann, A. S., de Fleury, M., Gbetkom, P. G., Calmettes, B., & Calmant, S. (2023). Water Resources in Africa under Global Change: Monitoring Surface Waters from Space. *Surveys in Geophysics*, *44*(1), 43–93. https://doi.org/10.1007/s10712-022-09700-9

Rahimi, B., & Foelsche, U. (2024). Observing atmospheric rivers using GNSS radio occultation data. *Atmospheric Measurement Techniques Discussions*, *2024*, 1–40. https://doi.org/10.5194/amt-2024-81

Ramos, A. M., Blamey, R. C., Algarra, I., Nieto, R., Gimeno, L., Tomé, R., Reason, C. J. C., & Trigo, R. M. (2019). From Amazonia to southern Africa: atmospheric moisture transport through low-level jets and atmospheric rivers. *Annals of the New York Academy of Sciences*, *1436*(1), 217–230. https://doi.org/https://doi.org/10.1111/nyas.13960

Ramos, A. M., Trigo, R. M., Tomé, R., & Liberato, M. L. R. (2018). Impacts of Atmospheric Rivers in Extreme Precipitation on the European Macaronesian Islands. *Atmosphere*, *9*(8). https://doi.org/10.3390/atmos9080325

Rautela, K. S., Singh, S., & Goyal, M. K. (2024). Characterizing the spatio-temporal distribution, detection, and prediction of aerosol atmospheric rivers on a global scale. *Journal of Environmental Management*, *351*, 119675. https://doi.org/https://doi.org/10.1016/j.jenvman.2023.119675

Reason, C. J. C. (2001). Subtropical Indian Ocean SST dipole events and southern African rainfall. *Geophysical Research Letters*, *28*(11), 2225–2227. https://doi.org/https://doi.org/10.1029/2000GL012735

Salimi, S., Helali, J., Lotfi, M., Momenzadeh, H., Hosseini, S. A., Asaadi Oskuei, E., Izadi, A., Yarmoradi, Z., & Bakhshi, I. (2020). Investigating the origin and pathways of atmospheric rivers in the world. *Theoretical and Applied Climatology*, *142*(1), 165–175. https://doi.org/10.1007/s00704-020-03299-w

Shao, X., Ho, S.-P., Jing, X., Zhou, X., Chen, Y., Liu, T.-C., Zhang, B., & Dong, J. (2023). Characterizing the tropospheric water vapor spatial variation and trend using 2007–2018 COSMIC radio occultation and ECMWF reanalysis data. *Atmospheric Chemistry and Physics*, *23*(22), 14187–14218. https://doi.org/10.5194/acp-23-14187-2023

Steiner, A. K., Lackner, B. C., Ladstädter, F., Scherllin-Pirscher, B., Foelsche, U., & Kirchengast, G. (2011). GPS radio occultation for climate monitoring and change detection. *Radio Science*, *46*(6). https://doi.org/https://doi.org/10.1029/2010RS004614

Traxl, D. (2022). *ARtracks - a Global Atmospheric River Catalogue Based on ERA5 and IPART (1.0.0) [Data set]. Zenodo.*

University Corporation for Atmospheric Research. (2024, September 12). *CDAAC: COSMIC Data Analysis and Archive Center*.

Vaquero-Martínez, J., & Antón, M. (2021). Review on the Role of GNSS Meteorology in Monitoring Water Vapor for Atmospheric Physics. *Remote Sensing*, *13*(12). https://doi.org/10.3390/rs13122287

Wang, S., Ma, X., Zhou, S., Wu, L., Wang, H., Tang, Z., Xu, G., Jing, Z., Chen, Z., & Gan, B. (2023). Extreme atmospheric rivers in a warming climate. *Nature Communications*, *14*(1), 3219. https://doi.org/10.1038/s41467-023-38980-x

Wentz, F. J., Hilburn, K. A., & Smith, D. K. (2012). *SSMI / SSMIS: Vol. Version 7*. Remote Sensing Systems.

Xu, G., Ma, X., Chang, P., & Wang, L. (2020). Image-processing-based atmospheric river tracking method version 1 (IPART-1). *Geoscientific Model Development*, *13*(10), 4639–4662. https://doi.org/10.5194/gmd-13-4639-2020

Zhu, Y., & Newell, R. E. (1994). Atmospheric rivers and bombs. *Geophysical Research Letters*, *21*(18), 1999–2002. https://doi.org/https://doi.org/10.1029/94GL01710

LIST OF FIGURES

APPENDIX

remote sensing

MDPI

Article

Atmospheric Rivers in Africa observed with satellite and reanalysis data

Linda Martina Maier [1*], Bahareh Rahimi [1] and Ulrich Foelsche [1,2]

[1] Institute of Physics, Department of Astrophysics and Geophysics (AGP), University of Graz, Austria
[2] Wegener Center for Climate and Global Change (WEGC), University of Graz, Austria
[*] *Correspondence to:* Linda Martina Maier (linda.martina.maier@gmail.com)

Abstract: Atmospheric rivers (ARs) transport significant amounts of moisture and cause extreme precipitation events, yet their behavior over Africa is not well understood. This study addresses this gap by analyzing the occurrence, seasonal variability, and spatial dynamics of ARs across the continent from 2009 to 2019. Utilizing ERA5 reanalysis data, Global Navigation Satellite Systems Radio Occultation (GNSS RO) measurements, and the Image-Processing-based Atmospheric River Tracking (IPART) method, distinct seasonal AR patterns are identified. Southern Africa experiences peak activity during austral summer, while AR occurrence in Northern Africa peaks in boreal winter and spring, aligning with regional rainy seasons. Moisture sources include the Atlantic Ocean, the Arabian Sea, and the Red Sea. The moisture transport is influenced by atmospheric dynamics such as shifts in the Intertropical Convergence Zone or El Niño Southern Oscillation (ENSO). Comparing ERA5 Integrated Water Vapor (IWV) estimates with high-resolution RO data revealed that ERA5 effectively captures broad-scale moisture patterns, but consistently reports higher IWV values compared to RO data, highlighting ERA5's tendency to represent a wetter atmosphere and RO's drier retrievals, particularly due to RO's underrepresentation of water vapor in the lower layers. Understanding AR dynamics in Africa is essential to improve climate resilience, water management and understanding extreme precipitation events.

Keywords: Atmospheric Rivers (ARs), Africa, ERA5 Reanalysis, GNSS Radio Occultation, IPART, ARtracks, Integrated Water Vapor (IWV)

Citation: To be added by editorial staff during production.

Academic Editor: Firstname Lastname

Received: date
Revised: date
Accepted: date
Published: date

1. Introduction

Atmospheric Rivers (ARs) are long, narrow corridors of concentrated water vapor that transport moisture over long distances. They are defined by a maximum width of 500 km and a minimum length of 2,000 km in the (lower) troposphere. Typically ARs are defined by tresholds, for Integrated Vapor Transport (IVT) this values need to be above 250 kg m^{-1} s^{-1}. Each AR can carry water vapor quantities comparable to the flow of the Mississippi River, with three to five events typically present per hemisphere at any time [1]. Known for influencing precipitation, ARs are responsible for heavy rainfall and flooding, particularly in mid-latitude and subtropical regions [2]. While AR dynamics are well-studied in America and Europe, studies in Africa remain limited. Globally, ARs are crucial in the hydrological cycle, contributing to water availability and extreme weather events. Their ability to transport large volumes of water vapor from tropical oceanic sources to inland areas has broad implications for water resource management, forecasting extreme weather and recognizing climate impacts [3]. Understanding their role in such processes underscores the importance of an in-depth understanding of AR characteristics specific to Africa, where weather patterns are uniquely complex.

1.1. Atmospheric Rivers Over Africa – Moisture Sources

In Africa, ARs influence rainfall patterns but have primarily been studied on a case-by-case basis, with limited research examining their behavior over an extended period across the entire continent. Key moisture sources for African ARs include the North and South Atlantic Ocean, the Arabian Sea, and the Red Sea [4, 5]. The North Atlantic Ocean plays a particularly important role in AR formation, as water vapor is transported eastward towards Africa, influencing rainfall in regions such as the Middle East and Northern Africa (MENA). In Southern Africa, ARs typically draw moisture from the South Atlantic Ocean and tropical areas, interacting with extratropical cyclones and cold fronts to produce heavy rainfall.

The occurrence of ARs over Africa is shaped by key factors, including moisture sources and atmospheric dynamics. A source of water vapor, like an ocean or sea, provides essential moisture, while large-scale pressure systems, such as cyclones, help organize this moisture into narrow vapor corridors. Wind shear, often generated by jet streams, maintains the elongated structure of ARs and drives rapid moisture transport [6].

The North Atlantic plays a particularly important role in AR formation for Northern Africa, Egypt and the Middle East, as moisture rich air is transported eastward, impacting rainfall in regions like Mauritania and Egypt [4]. In the Northern Hemisphere, the subtropical jet stream around 30°N transports tropical moisture toward higher latitudes, where it interacts with cyclonic systems to form ARs [7]. The interaction between upper-level cyclonic systems and mid-level anticyclonic circulations is essential for AR formation. Anticyclonic patterns over the Arabian Sea increase northward moisture transport from the Gulf of Aden and the Red Sea. In Africa, the merging of the subtropical and polar jet streams creates a stronger meridional flow, moving moisture inland more effectively [5]. In Northern Africa, ARs are influenced by the North Atlantic Oscillation (NAO). A positive NAO phase strengthens westerlies, pushing ARs farther inland, reaching Mauritania, Senegal, and the Middle East, with the subtropical and polar jet streams enhancing moisture transport [4].

In Southern Africa, ARs draw moisture from the South Atlantic and tropical sources, interacting with extratropical cyclones and cold fronts to deliver substantial rainfall, especially during winter [8]. The analysis by Ramos et al. (2018) [8] identifies four main moisture sources: (1) the western South Atlantic near Brazil, where tropical convergence enhances moisture uptake; (2) the eastern South Atlantic near the Cape Agulhas, linked to the Agulhas Current retroflection; (3) the Agulhas Current itself, which supplies a steady moisture stream along South Africa's east coast; and (4) continental sources in northern and northwestern South Africa, Namibia, and The Republic of Botswana. This moisture transport is further intensified by the South American Low-Level Jet (SALLJ), which channels Amazonian moisture to the South Atlantic, reinforcing AR-driven rainfall in Southern Africa. The pathways are shaped by the South Atlantic Subtropical High (SASH) and interactions with extratropical cyclones and cold fronts [7]. These ARs move along a southwest-to-northeast path, drawing moisture from the South Atlantic and occasionally from South America. In addition, mountain ranges intensify AR-driven precipitation through orographic lift, like the Cape Fold Mountains [8].

There they contribute to winter rainfall, since ARs are most common in early austral winter (May to September) [7, 9, 10]. For instance, Blamey et al. (2018) [7] observed that atmospheric rivers were responsible for approximately 70% of the 50 most extreme winter rainfall events, emphasizing their role in contributing to heavy rainfall and flooding risks.

1.2. Seasonal and Interannual Variability

ARs in both Northern and Southern Africa are subject to seasonal and interannual variability, largely driven by the interactions between global climate oscillations and regional weather patterns. In Northern Africa, AR activity peaks during the boreal fall and winter, when the Azores High retreats, allowing more moisture-laden air to penetrate the region [4]. Conversely, during the boreal summer, AR activity decreases due to the dominance of the Azores High and stable atmospheric conditions.

In Southern Africa, AR activity is highly seasonal, peaking during the austral winter (May to September), with extratropical cyclones and cold fronts driving moisture from the South Atlantic toward the southwestern coast of South Africa [8]. The interannual variability of ARs is further influenced large-scale climate patterns, including El Niño-Southern Oscillation (ENSO) and the Southern Annular Mode (SAM), which affect both the frequency and intensity of ARs across the African continent [11].

1.3. *Societal Relevance*

Water resource variability is a critical concern in Africa, especially for agriculture. With the continent's growing population climate-driven water variability poses a significant risk. Understanding patterns that lead to flooding is vital for planning climate resilience, especially in regions prone to extreme weather events [12]. With the increasing intensity and frequency of these events, integrating AR dynamics into climate adaptation strategies will be crucial for safeguarding communities and infrastructure [13]. Papa et al. (2023) [13] thus emphasizes the role of satellite monitoring for better forecasting, which can improve water management for agricultural productivity. In regions heavily reliant on seasonal rainfall, like sub-Saharan Africa, such forecasting tools are essential for climate adaptation and risk management. Enhanced atmospheric and climate research will support more effective public health interventions, sustainable agriculture, and resilient infrastructure, reinforcing the continent's capacity to respond to climate challenges. Investing in weather and climate service infrastructure in space is therefore another priority. This infrastructure is vital for improving daily safety and maintaining the technology that modern societies rely on [14]. Furthermore, ARs contribute to extreme weather events, including floods, which impact both water availability and health. Dezfuli et al. (2021) [15] highlight the role of AR-induced precipitation in the Middle East, where it not only affects water resources but also influences dust transport, impacting air quality and health in downstream regions. Similar effects are seen in West Africa, where dust exposure worsens respiratory and other health conditions. This underscores the need for localized studies to mitigate impacts and improve public health [16].

Together, these studies highlight the importance of advancing atmospheric research in Africa to address critical societal needs, from public health and water management to climate resilience and technological stability.

1.4. *Research Gaps and Objectives*

ARs are increasingly acknowledged as drivers of weather events in Africa, particularly during the winter seasons, contributing to extreme rainfall and flooding [17, 18, 19, 20]. Despite growing recognition of their impact, there remains a knowledge gap regarding the behavior of ARs in Africa. Specifically, the mechanisms of moisture transport within ARs and their interactions with local climate systems are not well understood. While extensive studies have focused on AR dynamics in regions such as America and Europe, relatively few analyses have been conducted across the African continent.

Our study addresses this gap by investigating AR events over Africa from 2009 to 2019. Utilizing the Image-Processing-based AR Tracking (IPART) method, this research seeks to identify AR patterns and assess seasonal and interannual variability across Northern and Southern Africa. To improve data accuracy, we compared ERA5 IWV measurement against Global Navigation Satellite Systems Radio Occultation (GNSS RO) data. These data were chosen because of their global coverage, high vertical resolution and stability over time. GNSS RO provides consistent atmospheric profiles unaffected by clouds or precipitation [21, 22]. This comparison aims to validate the reliability of ERA5 in capturing moisture levels associated with ARs. Our study aims to deepen the understanding of AR dynamics and their influence on Africa to improve climate resilience and water resource management in the region.

2. Materials and Methods

2.1. Data

The ERA5 reanalysis dataset, providing detailed historical climate data, supports hourly tracking of atmospheric parameters. Complementing this, GNSS RO data offers vertical moisture profiles, essential for understanding distinctive layers. IPART, an image-processing-based technique, refines AR tracking over land. The ARtracks catalogue, combining ERA5 and IPART, aids in identifying precise AR landfall locations.

The study period of 2009–2019 was selected as it provides a widespread timeframe to assess AR dynamics over Africa. This allows for an in-depth analysis of variability, supported by high-resolution dataset. The availability of high-quality, spatially and temporally detailed data during this period ensures accurate tracking and analysis of AR patterns. This timeframe strikes an effective balance between data reliability and the ability to capture trends, forming a solid foundation for examining AR contributions to Africa's hydrological cycle.

2.1.1. ERA5 reanalysis

The ERA5 reanalysis dataset from the Copernicus Climate Change Service (C3S) was used for interpolating and comparing with RO data. Data was drawn from the ERA5 hourly dataset available through the Climate Data Store (CDS), specifically focusing on Total Column Water Vapor (TCWV) to capture AR landfall events (https://www.ecmwf.int/en/forecasts/dataset/ecmwf-reanalysis-v5, last access: 03.10.2024) [23]. With a 0.25° spatial resolution and hourly data, ERA5 provides high-quality historical records dating back to 1940.

ERA5 integrates observational data from multiple sources (e.g., satellites, radiosondes) with model data using the European Centre for Medium-Range Weather Forecasts (ECMWF) Integrated Forecast System and 4D-Var data assimilation. This combination enhances accuracy and consistency across the time series, supported by precise quality control to ensure reliable results [24].

2.1.2. GNSS Radio Occultation Data

Additionally, reprocessed Level 2 RO data from multiple satellites: TerraSar-X (TXS), Gravity Recovery and Climate Experiment (GRACE), Constellation Observing System for Meteorology, Ionosphere, and Climate-1 (COSMIC-1, 6 satellites), Meteorological Operational Satellites (Metop series), PAZ and the Korean Multi-Purpose Satellite-5 (Kompsat 5). We obtained the data through the COSMIC Data Analysis and Archive Center (CDAAC) (https://data.cosmic.ucar.edu/gnss-ro/, last access: 03.10.2024). This dataset provides profiles of temperature, pressure, and humidity [25]. This RO technology measures atmospheric refractivity by detecting the bending of GNSS signals as they pass through the atmosphere, influenced by variations in altitude, temperature, pressure, and humidity. Bending angles derived from these measurements are used to construct vertical profiles, capturing the atmospheric structure with high resolution. This enables profiling of atmospheric layers, particularly in the lower atmosphere, where RO achieves resolutions of about 0.1 km near the surface [26]. GNSS-RO data have first been used for accurate monitoring of atmospheric temperature in the upper troposphere and lower stratosphere (e.g., [27, 28]). However, the potential for observing water vapor in the (lower) troposphere has already been recognized in the 1990s (e.g., [29, 30]) and GNSS RO data are increasingly used for observing water vapor (e.g., [31, 32]), even under particularly dry conditions [33]. GNSS-RO data have already been successfully used to observe ARs (e.g., [34, 35]), and the assimilation of GNSS-RO data has been demonstrated to improve AR forecasts [36]. The dataset used in our study thus provides detailed vertical moisture profiles, global coverage and all-weather capability crucial for tracking atmospheric changes [22].

Analysis of this dataset by Rahimi and Foelsche (2024) [21] highlights the tendency of RO to underestimate IWV when compared with independent measurements from the Special Sensor Microwave Imager/Sounder (SSMI/S), a satellite-based instrument that provides global IWV observations with a horizontal resolution of 25-50 km. SSMI/S measures thermally emitted microwave radiation, making it especially reliable over oceans where surface emissivity is uniform. While CDAAC and WEGC show strong agreement in their GNSS-RO-derived moisture profiles, despite using different retrieval methodologies, the study reveals that GNSS-RO IWV values are approximately 85% of SSMI/S values. Since RO data generally do not capture humidity in the lowest few hundred meters of the atmosphere, this systematic difference can be largely attributed to RO. Comparisons between WEGC GNSS-RO profiles and ECMWF background data further show close alignment (~95%), while both datasets remain significantly drier than ERA5 [21].

2.1.3. Image-Processing-based Atmospheric River Tracking

The IPART method is used to identify and analyze AR events across Africa. Developed by Xu et al. (2020) [37], IPART enhances AR detection by focusing on the spatial and temporal characteristics of ARs rather than relying solely on threshold values for Integrated Water Vapor (IWV) or Integrated Vapor Transport (IVT), which are common in traditional methods (https://github.com/ihesp/IPART, last access: 14.11.2024).

At the core of IPART is the Top-Heat by Reconstruction (THR) algorithm, a technique from image processing that identifies moisture structures even in noisy data, highlighting regions of high moisture continuity. The THR algorithm operates through steps like greyscale erosion and dilation, emphasizing key moisture areas, which are then mapped to identify ARs. The method constructs a topological graph of the AR's moisture flow, accurately tracking the AR’s central path or “axis” as it progresses [37].

ARtracks

The ARtracks catalogue, a global resource combining ERA5 reanalysis data with IPART, was used to locate AR landfall points. ARtracks supports the detection, visualization, and tracking of AR events, providing a detailed AR axis path and landfall location based on IVT and other meteorological data [38]. This catalogue helps with precise analyses of AR impact patterns and their geographic extent (https://github.com/dominiktraxl/artracks, last access: 14.11.2024).

2.2. *Data Preprocessing and Quality Control*

To ensure accuracy and consistency across datasets, this section outlines the data preparation steps for analysis over the African continent. The study centers on two main analytical objectives: (1) statistical analysis of AR occurrences, highlighting regional and seasonal trends, and (2) interpolation and comparison of moisture data between RO observations and ERA5 reanalysis. The preprocessing pipeline is structured to maintain data integrity, consistency, and relevance for both objectives.

2.2.1. Statistical Analysis of AR events over Africa

In the initial analysis, ARtracks data from 2009 to 2019 was processed to capture the spatial and temporal characteristics of AR landfalls impacting Africa. Preprocessing involved formatting timestamps, filtering by geographic boundaries, and categorizing events by region (Northern and Southern Africa) to allow for detailed seasonal and regional comparisons. The dataset was organized by year and month, enabling analysis of annual and seasonal trends. Filtering retained only AR events within a custom-defined African boundary, excluding areas like the Arabian Peninsula. Landfall points were verified using the Python Shapely library, ensuring that only events within Africa were included.

Each AR event was classified as either Northern or Southern Africa based on latitude, facilitating regional impact comparisons. This North-South division allows a comparative analysis across Africa's diverse climates, with Northern Africa influenced by Saharan and Mediterranean patterns, while Southern Africa interacts with moisture sources from the Indian and Atlantic Oceans. Quality control steps included date-time formatting for consistent filtering, removal of missing or duplicate entries, and verification of landfall coordinates to maintain spatial accuracy.

2.2.2. Interpolation and Comparison of RO and ERA5 Data

In the second part of the analysis, moisture data from RO observations were compared with ERA5 reanalysis data to validate moisture transport estimates and evaluate ERA5 performance. Given differing spatial and temporal resolutions, interpolation and alignment steps ensured synchronization. ERA5 data (latitude, longitude, time, and Total Column Water Vapor (TCWV)) were formatted uniformly, while RO data were cleaned to ensure numeric values in the IWV column and remove incomplete records. Domain-specific knowledge was applied by ensuring valid values at 1 km altitude, filtering invalid values and validating the geographic domain to minimize errors and outliers.

A nearest-neighbor search matched ERA5 points with RO coordinates, and temporal interpolation estimated ERA5 IWV values at RO observation times, weighting nearby grid points by distance (see chapter 2.3.2.1.). To ensure alignment, only ERA5 data within a 2.5° spatial and 3-hour temporal range of RO observations were retained. Both datasets were checked for matching units, non-numeric entries were converted to NaN, and outliers were reviewed to prevent bias.

2.3. *Methodology*

The methodology for analyzing AR occurrences over Africa and validating ERA5 reanalysis data with RO observations is outlined here. First, the IPART method, combined with the ARtracks catalogue, is applied to detect, visualize, and statistically analyze AR frequencies and patterns, with a focus on seasonal and regional variations across Africa. Second, a comparative analysis between ERA5 and RO data assesses the accuracy of the reanalysis data in capturing moisture transport, utilizing interpolation and statistical metrics to quantify deviations.

2.3.1. Statistical Analysis of AR Occurrence over Africa

The IPART method was used to analyze IVT anomalies associated with ARs over Africa. Seasonal IVT averages from ERA5 were calculated to identify elevated moisture periods, with anomalies defined as percentage deviations from climatology baselines. The ARtracks catalogue provided data on AR occurrences and seasonality from 2009 to 2019, filtered to include only landfalls within Africa, categorized by Northern or Southern Africa based on centroid latitude. Visualizations, including bar charts, line graphs, and heatmaps, display annual, monthly, and seasonal AR patterns across these regions, as detailed in chapter 3.

To assess frequency and trends, AR events with axes extending toward the continent were prioritized. Africa's boundaries were defined using a custom polygon in Shapely, with Cartopy confirming AR landfalls within these limits. This filtering ensured that only

AR events relevant to Africa were analyzed. Additional data for the Arabian Peninsula was later included for the research on the MENA region (chapter 2.3.2.).

Integrated Vapor Transport (IVT)

The ARtracks catalogue data includes each AR event's date, duration, landfall location, average IVT value, and IVT-weighted centroid coordinates, useful for tracking AR movement. Centroids, calculated from IVT vectors (combining wind and specific humidity), represent the AR's central moisture transport path. They represent the central location of the water vapor transport within the AR. IVT is measured in kg m^{-1} s^{-1} and it quantifies the amount of water vapor moving through the atmosphere over a certain distance each second. Comparing the IVT to a phenomenon on the ground, IVT equals the flow rate of a river [39]. High IVT values indicate strong moisture transport linked to heavy precipitation.

The IVT is calculated as follows:

$$IVT = \sqrt{\left(\frac{1}{g}\int_{p_s}^{p_t} qu\, dp\right)^2 + \left(\frac{1}{g}\int_{p_s}^{p_t} qv\, dp\right)^2} \quad (1)$$

where q is specific humidity, u and v are the zonal and meridional wind components, p_s and p_t are surface and top-of-atmosphere pressures, and g is the acceleration due to gravity. This vertical integration captures the total atmospheric moisture transport associated with ARs.

2.3.2. Comparative Analysis using RO and ERA5 reanalysis data

The validation of ERA5 reanalyses with RO observations is divided into two parts: (1) interpolation of RO data to create continuous vertical profiles of atmospheric moisture and (2) direct comparison of these interpolated RO profiles with ERA5 data, aligned in space and time.

RO Interpolation – Inverse Distance Weighting

Inverse Distance Weighting (IDW) interpolation generates continuous vertical profiles from discrete RO data points, producing smooth and accurate representations of atmospheric moisture. IDW is a spatial interpolation method where the value at an unsampled location is a weighted average of nearby known values and closer points are weighted stronger. The nearest neighbors are identified using a k-dimensional tree (KDTree) that retrieves the coordinates and distances to the closest 4 grid points that then serve as the basis for weighting the known values during the IDW:

$$\mathrm{F(s)} = \sum_{i=1}^{n} w_i z(s_i) = \frac{\dfrac{\sum_{i=1}^{n} z(s_i)}{|s - s_i|^P}}{\sum_{j=1}^{m} \dfrac{1}{|s - s_j|^P}} \quad (2)$$

$$w = \frac{1}{|s - s_x|^P} \quad (3)$$

where s is the unsampled location, $z(s_i)$ is the value at a known point, and $|s\text{-}s_x|$ represents the distance between the known and unknown points [40]. F is the interpolated value at position s and P controls the rate at which the weight decreases with distance. A power of 2 was chosen through literature review, it is optimal for climate data, as it balances the influence of nearer and farther points, providing a realistic spatial distribution [40, 41, 42, 43, 44].

Integrated Water Vapor

For interpolation, RO data from multiple satellite sources are used to calculate IWV by integrating temperature, vapor pressure, and pressure data from wet profiles on the day of the AR event. It is expressed in kilograms per square meter (kg m^{-2}) and the value is important to understand the role of water vapor in ARs, particularly for assessing precipitation potential and moisture transport. The unit represents the total amount of water vapor present in a vertical column of the atmosphere. IWV is calculated as follows:

$$\mathrm{IWV} = \frac{1}{g}\int_{p_s}^{p_t} q\,dp \tag{4}$$

Here, q is specific humidity, g is acceleration due to gravity, p_s and p_t are surface and top-of-atmosphere pressures, respectively.

The integral (equation 4) represents a continuous atmospheric column, while the sum (equation 5) approximates this for discrete pressure layers, where q_i is specific humidity at the i^{th} level and Δp_i is layer thickness [45, 46].

$$\mathrm{IWV} = \frac{1}{g}\sum_{i=1}^{n} q_i\,\Delta p_i \tag{5}$$

Specific humidity, however, is not directly provided in the CDAAC wet profiles, it was therefore calculated based on [21]. The equation for the specific humidity is given in equation 6 and equation 7.

$$q = \frac{\varepsilon \cdot p_v}{p \cdot p_v \cdot (1-\varepsilon)} \tag{6}$$

$$\varepsilon = \frac{M_w}{M_d} \tag{7}$$

The constant ($\varepsilon = 0.622$) represents the ratio of the molar mass of water vapor ($M_w = 18.015$ g mol^{-1}) to the molar mass of dry air ($M_d = 28.965$ g kg^{-1}) [47]. Profiles of vapor pressure p_v and total air pressure p are taken from the CDAAC wet profile data.

Comparative Analysis of RO and ERA5 Data

In the second part of the analysis, ERA5 reanalysis data were compared with RO satellite data (TXS, GRACE, COSMIC-1, Metop series, PAZ and Kompsat 5). The data were spatially and temporally interpolated to align with RO observation points, allowing a direct comparison. Interpolation was conducted using KDTree for nearest neighbors and IDW for spatial precision, with temporal interpolation aligning observation times to within a 2.5° spatial and 3-hour temporal range.

The datasets were then assessed using Mean Bias and Root Mean Square Error (RMSE) to quantify ERA5's performance, with RMSE values categorized as low (<10%), medium (10-30%), and high (>30%) relative to observed values, based on literature standards [48, 49, 50]. Lower RMSE indicated better alignment with RO data, while higher RMSE suggested greater discrepancies due to differences in atmospheric, spatial, or temporal factors.

2.4. Selected AR Events

We selected AR events spanning both the Northern and Southern Hemispheres from 2009 to 2019, covering austral spring and autumn as well as boreal spring and winter. The events were chosen for their geographic and seasonal diversity. Each event is documented in prior literature, confirming its classification as an AR. Table 1 includes each event's date that was chosen based on precipitation, affected region, study domain, and satellite sources used for RO observations.

Table 1. Investigated AR events from 2009 to 2019

Event name	Date	Affected region	Area	RO Satellites	Study domain (Lat°/ Lon°)
South Africa 2009	26.09.2009	West coast of South Africa	Southern Africa	Cosmic-1 Metop-A GRACE TSX	-10 to -50 / -40 to 30
MENA 2010	15.03.2010	MENA Region	Northern Africa	Cosmic-1 Metop-A TSX	45 to 10/ 0 to 60
Morocco 2010	30.11.2010	Morocco	Northern Africa	Cosmic-1 Metop-A GRACE TSX	45 to 10/ -45 to 15
South Africa 2013	26.05.2013	West coast of South Africa	Southern Africa	Cosmic-1 Metop-A Metop-B GRACE TSX	-5 to -45/ -40 to 30
MENA 2017	14.04.2017	Middle East/ Iran	Northern Africa	Cosmic-1 Metop-A Metop-B Kompsat5	50 to 10/ 10 to 60
Mauritania 2019	24.03.2019	Middle East	North Africa	Cosmic-1 Metop-A Metop-B TSX Kompsat5 PAZ	40 to 10/ -30 to 60

These events highlight key AR dynamics such as moisture uptake, long-distance transport, and interactions with geographic features that intensify precipitation impacts. The selected events, covering diverse regions and seasons, form a robust foundation for analyzing AR behavior across Africa. The study domains for each event are shown in Figure 1.

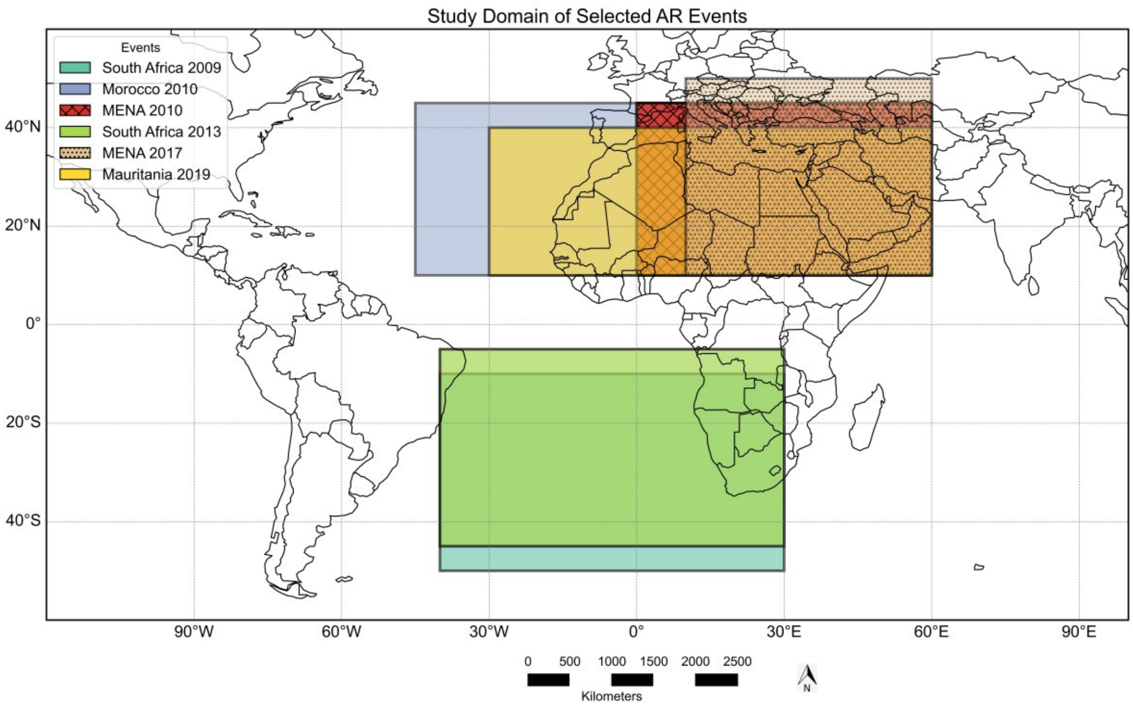

Figure 1. Study Domains of Selected Atmospheric River events

The **South African 2009** event affecting the west coast of South Africa in September 2009, occurred during austral spring. It showed unusual moisture uptake from regions typically outside Southern Africa's moisture sources, exemplifying teleconnections between South America and South Africa. The event notably impacted the Western Cape Province, which is especially vulnerable to ARs due to its closeness to the South Atlantic Ocean [21].

Taking place in March 2010, in the Middle East and North Africa (MENA) region, the **MENA 2010** event occurred in boreal spring. It influenced dust transport and interacted with snowmelt processes in the Near East highlands. The AR primarily drew moisture from the Red Sea and northeastern Africa, impacting the highlands of the Near East and making it a key event for studying AR influences during the snowmelt season [51].

In November 2010, an AR event brought intense rainfall to Morocco, causing substantial flooding, especially in urban areas like Casablanca. The **Morocco 2010** event produced precipitation levels nearing 180 mm at specific rain gauges, severely affecting infrastructure. Occurring in late boreal autumn, this event provides insight into North Africa's pre-winter climate conditions [17].

In the boreal winter of 2011, the **Mauritania 2011** event impacted East Sahara, Mauritania, Morocco, and Guinea. The AR demonstrates high frequency and extensive reach. ARs in this area are often influenced by upper-level jet streams, enabling long-distance moisture transport from the North Atlantic and Red Sea, bringing moisture across arid regions [4].

The **South Africa 2013** austral autumn event in May 2013, contributed to South Africa's winter rainfall, with intense northward moisture flow originating from the South Atlantic and moving toward South Africa. The interaction between a subtropical high-pressure system and a low-pressure system over the continent intensified the event, highlighting ARs' role in South African winter precipitation [7].

In April 2017, the **MENA 2017** AR event impacting the region, caused flooding and influenced snowmelt, especially in Iran. Moisture sources included the Red and

Mediterranean Seas, with effects on areas such as Lake Urmia. The event also carried Saharan dust, affecting precipitation and ecosystems across long distances [15].

Illustrating rapid shifts from drought to flooding, the **Mauritania 2019** event affected North Africa and the Middle East in March 2019. It resulted in severe flooding as far as Iran, causing extensive infrastructure damage and loss of life. This event exemplifies how climate extremes can intensify under changing climate conditions [5, 52].

3. Results and Discussion

This chapter presents the results of the (1) statistical analysis of AR events over Africa using IPART and ARtracks. ERA5 data accuracy against high-resolution RO measurements is evaluated with the (2) Comparison of RO and ERA5 data.

3.1. Statistical Analysis of AR Events over Africa

This section presents results from the IPART and ARtracks analysis, highlighting AR frequency, monthly distribution, and hemispheric differences across the continent. We identified 1,730 ARs impacting Africa between 2009 and 2019, with annual fluctuations shown in Figure 2. The number of ARs varies yearly, with the highest count in 2011 (174 ARs) and the lowest in 2009 (139 ARs). Overall, the number of ARs stays relatively constant over the period, shown by the annual average of 159 ARs.

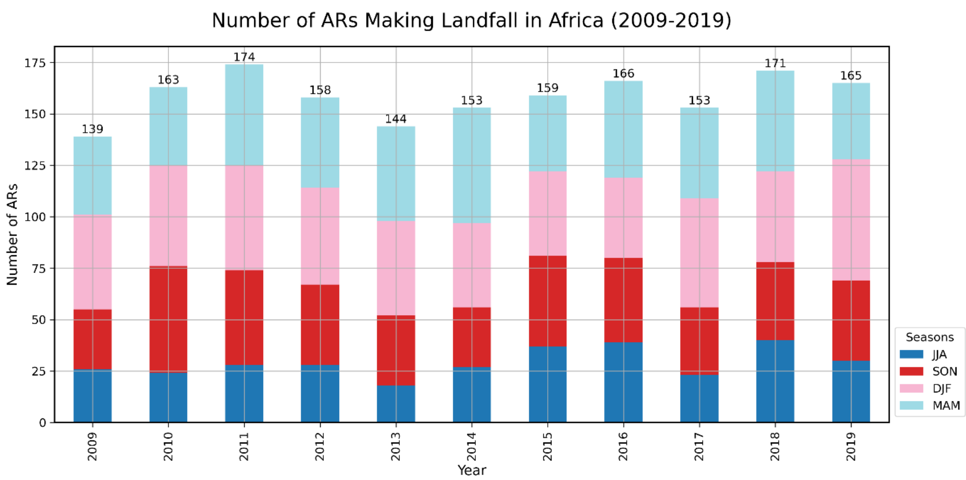

Figure 2. Total number of AR events each year filtered for respective seasons

Figure 2 illustrates both seasonal and interannual AR variability, showing event distribution by season each year. Austral summer (DJF: December, January, February; pink) and autumn (MAM: March, April, May; light blue) display higher AR frequencies than winter (JJA: June, July, August; dark blue) and spring (SON: September, October, November; red). The seasonal averages for AR activity were 29 (JJA), 39 (SON), 47 (DJF), and 44 (MAM).

Notably, the years 2011, 2016, 2018 and 2019 show elevated AR counts. The DJF season is the most active season, with a peak in 2019 (59) and a low in 2014 (41) and 2015 (41), while MAM shows a maximum in 2014 (56) and a minimum in 2015 (37) and 2019 (37). JJA consistently records the least AR activity ranging from 18 in 2013 to 40 in 2018, and SON exhibits moderate variability, with a peak in 2010 (51) and a low in 2009 (29) and 2014 (29).

To analyze potential correlations between the frequency of ARs and climatic conditions, we examined the ENSO 3.4 index, which measures sea surface temperature (SST) anomalies in the central equatorial Pacific Ocean and compared it to the number of ARs making landfall in Africa. This index is an indicator of El Niño and La Niña phases, with positive values indicating El Niño (warmer ocean temperatures) and negative values indicating La Niña (cooler ocean temperatures) [53]. Warm and cold phases happen when sea surface temperatures in the Niño 3.4 region are either warmer or cooler than normal by at least 0.5°C for five months in a row [54, 55, 56]. Some general patterns emerged from the comparison.

The El Niño years 2015-2016, marked by strong SST anomalies (up to +2.6°C in OND and NDJ 2015), agreed with increased AR activity in certain seasons, such as JJA (37 and 39 ARs respectively, both values above average) and SON (44 and 41 ARs) that were among the highest recorded for these seasons. The annual totals were 159 events in 2015 and 166 ARs in 2016.

During the study period La Niña conditions prevailed in 2010-2011 and 2017-2018, with the strongest phase observed in 2010-2011 (ENSO 3.4 index: -1.6 in SON 2010). Those years are generally associated with more variable AR activity during the seasons, showing the highest annual counts for the study period (174 in 2011 and 171 in 2018). While JJA activity was consistently low during La Niña due to a weakened subtropical jet (e.g., 24 ARs in 2010 and 23 in 2017), DJF remained relatively robust, as seen in 2011 (51 ARs) and 2017 (53 ARs). MAM activity during La Niña years also displayed variability, with high counts in 2011 and 2018 (49 ARs each). Notably is the activity in SON 2010 (52) showing the highest value of this season (corresponding to the lowest seasonal ENSO 3.4).

Neutral years, such as 2009, 2012-2014, and 2019, were characterized by ENSO 3.4 index values between -0.5 and +0.5. Those years show generally steady AR activity, with moderate MAM activity, but a notable exception in MAM 2014 (56 ARs, highest for the season). JJA counts are low, which is typical for that season (e.g., 26 ARs in 2009 and 18 in 2013).

Average monthly AR distributions from 2009 to 2019 reveal distinct patterns, with peak activity in January (188 ARs), February (181 ARs) and March (198 ARs), a second peak in October (163 ARs) and a minimum in July (85 ARs), as shown in Figure 3.

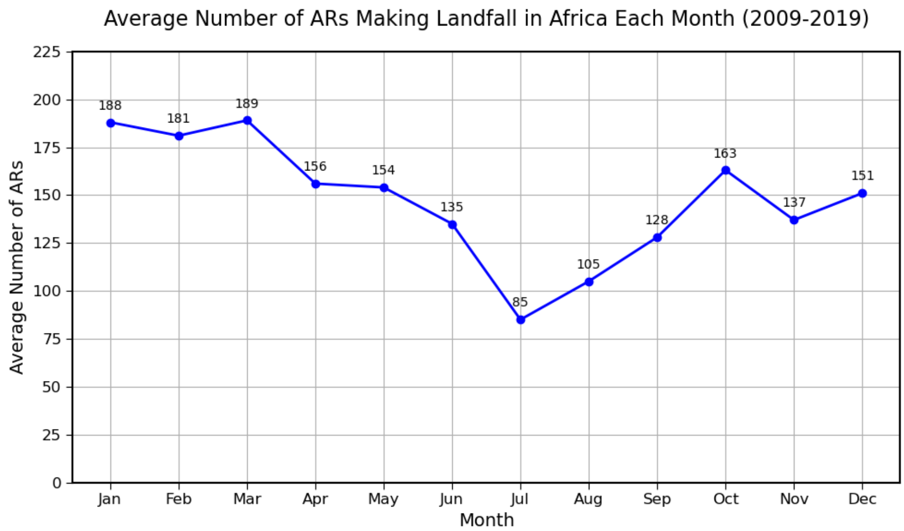

Figure 3. Average number of ARs making landfall over the period 2009-2019

AR activity gradually declines during April (156 ARs), May (154 ARs) and June (135 ARs) as the seasonal transition progresses into boreal summer. The heatmap in Figure 4 further highlights monthly AR frequencies, with darker shades indicating peak months.

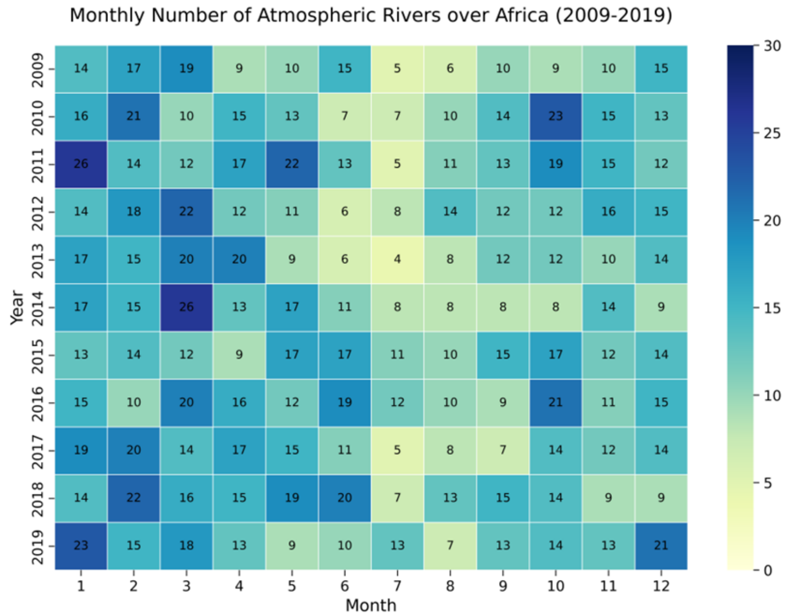

Figure 4. Heatmap - monthly number of ARs over the whole continent of Africa

Boreal winter and spring months consistently show more AR events across multiple years, consistent with the dominance of DJF as the most active season, with peaks such as January 2011 (26 ARs), February 2018 (22 ARs) or January 2019 (23 ARs) shown in Figure 2. MAM also shows elevated activity, with the highest monthly count of 26 ARs occurring in March 2014. In contrast, JJA consistently exhibits the lowest AR counts, with a minimum of 4 ARs in July 2013 during a neutral ENSO year.

3.1.1. Southern and Northern Africa

In the statistical analysis, AR activity was separated by hemisphere at the equator, with results shown in Figure 5 for landfalling ARs from January 2009 to December 2019. The chart displays monthly AR activity in Northern Africa (blue line) and Southern Africa (green line).

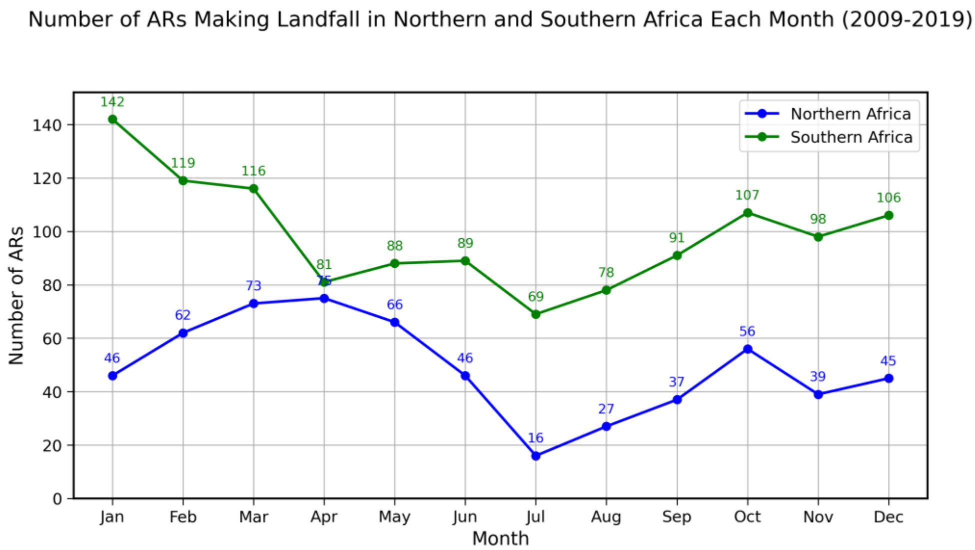

Figure 5. Number of ARs making landfall for each month for both hemispheres

Only ARs making landfall in Africa are included, excluding the Arabian Peninsula. Southern Africa shows consistently higher AR activity over the entire study period. Visible is a peak in January (142 ARs), high activity in February (119 ARs) and March (116 ARs) and a secondary peak in October (107ARs). In Northern Africa high AR counts are observed from February (62 ARs) to May (66 ARs) with a secondary peak in October (56 ARs) and minimal activity in summer, aligning with the study by Francis et al. (2022) [57], which highlights AR-driven moisture transport toward Europe.

In both regions a minimum activity is shown in July (Southern Africa: 69 ARs, Northern Africa: 16 ARs). Additionally, there is a secondary peak visible in October (Southern Africa: 107 ARs, Northern Africa: 56 ARs). The following sections provide a more detailed analysis of each region, with additional charts for further insight.

While Figure 5 shows the seasonality of AR landfalls in Southern Africa, where AR activity remains consistently higher than in Northern Africa, Figures 6 and 7 give a more detailed visualization on annual differences. It presents a heatmap of monthly AR activity over Southern Africa.

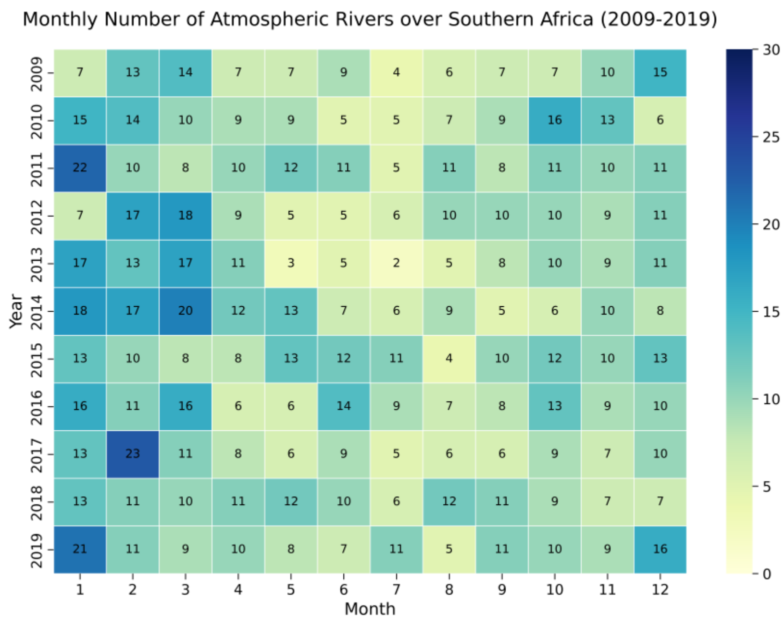

Figure 6. Heatmap - monthly analysis ARs over Southern Africa

Comparing Figure 5 and 6, AR activity is relatively high from October to March (see Figure 5 and 6), but strong activity is observed from January to March, with highest peaks in January (e.g., 22 ARs in 2011 or 21 ARs in 2019) and February 2017 (23). In contrast, austral winter months (JJA) show minimal AR activity, with July typically recording the fewest events (e.g., only 2 in July 2014). This seasonal pattern underscores the role of ARs in Southern Africa's wet season, contributing to summer precipitation, while winter remains drier with reduced AR influence [7]. Year-to-year variation is again evident, with higher AR activity in years like 2014 and 2019 and lower counts in 2009 and 2013, indicating sensitivity to large-scale atmospheric dynamics.

Although literature (e.g., [58]) often reports peak AR activity during austral winter (May-September), the 2009-2019 data show prominent activity during austral summer (DJF) and autumn (MAM), aligning with the region's summer rainy season but diverging from some previous findings [6, 7, 59]. Our differing findings may stem from the limited existing research on Southern African ARs. Although our study period is comparatively short, we found noteworthy results, including the average number of 158 ARs per year and a small variation in the absolute number of landfalling ARs per year.

Northern Africa, situated between the subtropics and mid-latitudes, experiences most AR activity during boreal winter (DJF), with lower overall frequency compared to Southern Africa. AR patterns are driven by mid-latitude low pressure systems that transport moisture from the Atlantic, crucial for this arid region's water supply [5].

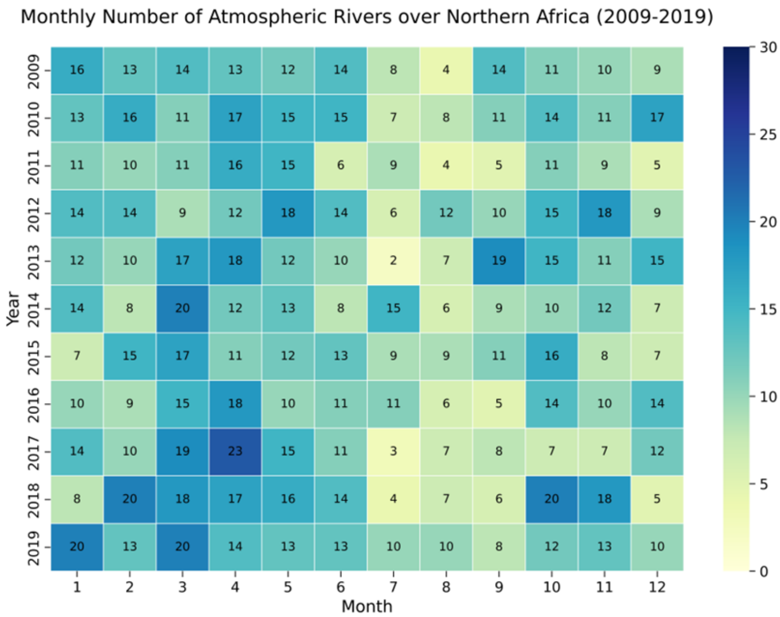

Figure 7. Heatmap - monthly analysis ARs over Northern Africa

Figure 7 shows monthly AR trends in Northern Africa. Boreal winter (DJF) and spring (MAM) months again show higher AR frequency, contributing to precipitation, with peaks in January 2019 (20 events), April 2017 (23 events), or March 2014 and 2019 (20 events). Conversely, summer (JJA) and early autumn (SON) show minimal AR activity, with July typically showing the lowest AR activity.

Research [19, 52, 58, 60] confirms that ARs peak in boreal autumn and winter, supporting critical precipitation during these seasons: This AR variability is also influenced by shifts in the Intertropical Convergence Zone (ITCZ), leading to a marked decrease in mid-year AR occurrences [4, 18].

3.2. *Comparison of RO and ERA5 Data*

Here we examine the relationship between IWV values from GNSS RO and ERA5 reanalysis data through case studies of six representative AR events in regions like Southern Africa, Middle East and North Africa (MENA), and West Africa. Through analysis of regression lines, Mean Biases, and RMSE, we assess ERA5´s accuracy against high-resolution RO data. It is important to note that while RO data possess high vertical resolution, they tend to underestimate IWV due to reduced sensitivity in the lower troposphere—a limitation contributing to the underestimation of IWV (as previously discussed).

Scatter plots and geospatial maps are utilized to compare IWV values from the two datasets at corresponding locations and times. The scatter plots illustrate the alignment between datasets, highlighting patterns and discrepancies. The red dashed line represents perfect alignment between ERA5 and RO datasets, while the green regression line denotes the line of best fit. Geospatial maps visualize the spatial distribution of moisture, enabling the identification of regions with consistent agreement and areas with notable deviations

3.2.1. South Africa 2009 event

This event delivered moisture from the South Atlantic and remote sources like South America to South Africa, causing extreme rainfall at the Western Cape [8]. The scatter plot (Figure 8 (a)) shows a high number of RO events (131) and a wide IWV range of ~3 to 43 kg m^{-2}, reflecting strong moisture transport. A spread in the data is evident at higher IWV values. At lower IWV values, below ~10 kg m^{-2}, a good agreement between the RO data and the interpolated ERA5 IWV values is visible, as indicated by the close alignment of the data points (blue) the regression line (green). This comparison yields in an RMSE of 4.37 kg m^{-2}. The Mean Bias is -2.01 kg m^{-2} and together with the regression line slope of 0.82 this event indicates the tendency for ERA5 to show wetter data relative to GNSS RO. Former findings by Rahimi and Foelsche (2024), support this finding, that prevail throughout all events.

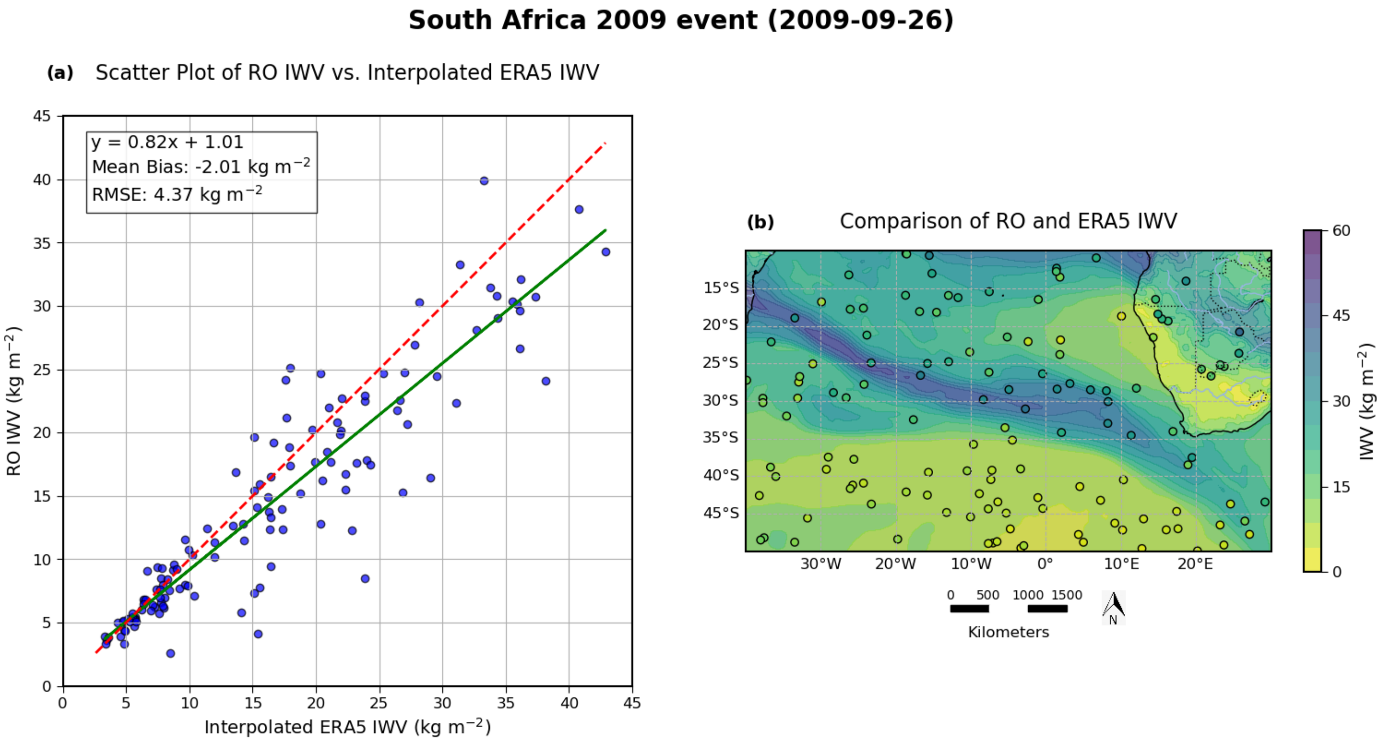

Figure 8. Analysis of the Southern Africa 2009 event. **(a)** Scatter plot of Radio Occultation (RO) versus ERA5 Integrated Water Vapor (IWV). **(b)** Map showing IWV from ERA5 (background) and from RO (filled circles). Scale reverse to the center latitude.

The spatial map (Figure 8 (b)) visualizes ERA5 IWV distribution overlaid with RO measurements (filled circles) and demonstrates the capability of the reanalysis dataset to capture large-scale moisture transport patterns associated with the AR event. The filled circles represent the IWV values from the RO observations. The scale on the color bar indicates IWV values with yellow and green indicating lower and blue indicating higher values. The IWV values derived from the RO dataset are represented by the black-edged circles. Discrepancies in color indicate differences between the two data sets. In high-moisture areas ERA5 shows higher IWV than RO, highlighting its tendency to exhibit a positive bias in regions with finer-scale moisture variations. On the edges of AR events higher discrepancy is expected due to sharp humidity gradients.

3.2.2. MENA 2010 event

Occurring during boreal spring, this AR event highlights the impact of AR on snowmelt and dust transport in the MENA region [51].

The IWV range in Figure 9 (a) (~2 to 32 kg m^{-2}) is characteristic of moderate moisture transport typical of weaker ARs (also evident in Figure 9 (b)). The data points are tightly clustered around the regression and 1:1 line, indicating minimal systematic bias and variability. This is indicated by the lowest RMSE amongst all events at 3.11 kg m^{-2}, and the smallest Mean Bias of -1.61 kg m^{-2}. This relationship between the CDAAC RO and interpolated ERA5 IWV can be expressed by the equation y= 0.80x + 0.81, showing that RO values are about 80% of the ERA5 values.

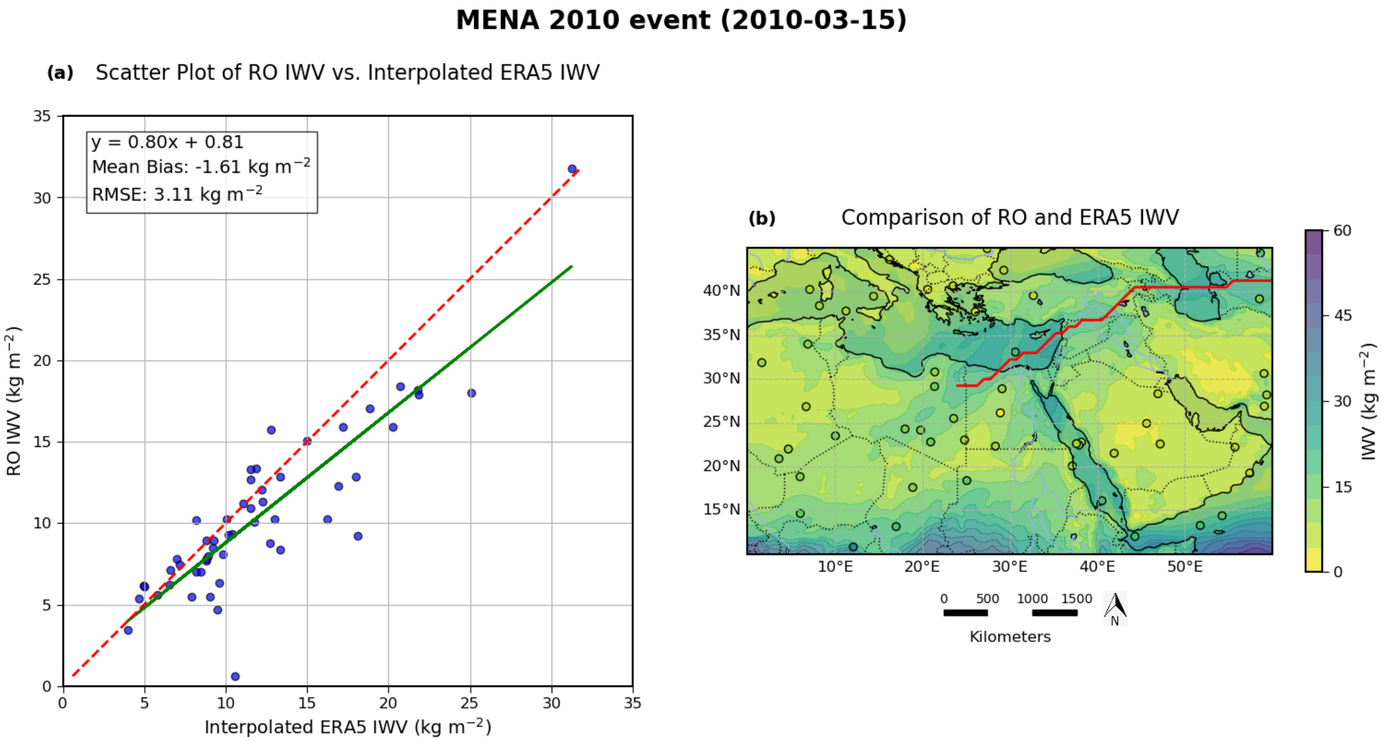

Figure 9. Analysis of the MENA 2010 event. **(a)** Scatter Plot of RO versus ERA5 IWV. **(b)** IWV from ERA5 (map) and from RO (filled circles) including the path of the AR (red).

The spatial map in Figure 9 (b) illustrates IWV patterns across the MENA region, with the red line indicating the path of the AR. The path is defined using data from the ARtracks catalogue (see chapter 2.1.3.1). High moisture areas are shown over the Red Sea and the Arabian Peninsula. ERA5 exhibits a positive bias of IWV in the eastern Mediterranean and northern Africa. Limited satellite observations over land reduce AR visibility for this specific event, though the AR pathway affects regions from the Arabian Peninsula to the Middle East.

3.2.3. Morocco 2010 event

The Morocco 2010 event was marked by extreme rainfall leading to widespread flooding and infrastructure damage [17]. The IWV in the scatter plot (Figure 10 (a)) spans ~7 to 52 kg m- ^{2}, underscoring the strong moisture transport associated with this AR, illustrate in Figure 10 (b). The Mean Bias of -2.33 kg m^{-2} (largest among all events) and RMSE of 4.41 kg m^{-2} reflect moderate discrepancies. For this event ERA5 values are 122% of the RO values, which is shown by the slope of 0.82 that is the same as in the South Africa 2009 event. However, the scatter of the sample size of RO observations (44) is smaller than in the 2009 event.

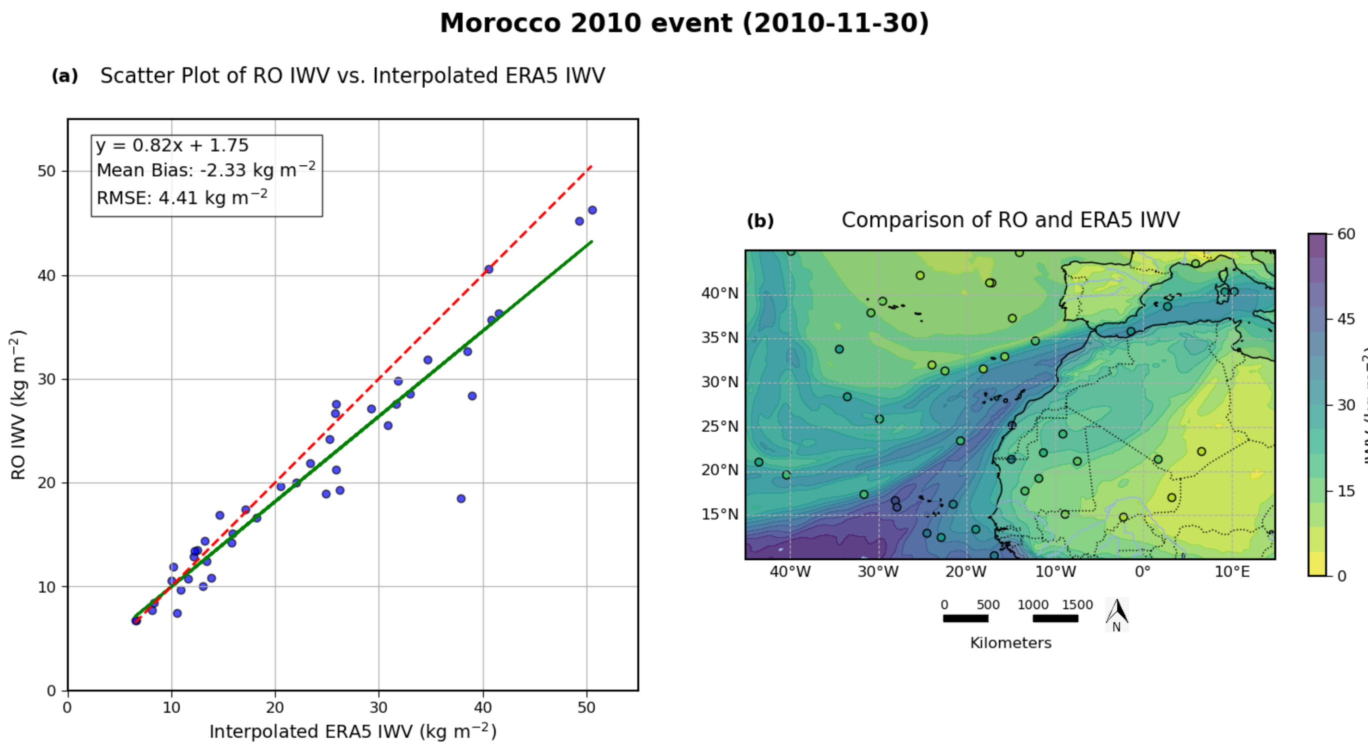

Figure 10. Analysis of the Morocco 2010 event. **(a)** Scatter Plot of RO versus ERA5 IWV. **(b)** IWV from ERA5 (map) and from RO (filled circles).

Figure 10 (b) illustrates high IWV over the Atlantic west of Morocco, captured well by ERA5, which shows extensive moisture transport toward the Moroccan coast. However, ERA5 reports systematically higher IWV levels in oceanic and northern Morocco regions compared to RO, that tends to retrieve drier profiles. IWV decreases inland, aligning well between datasets, though RO reports slightly lower values in some areas, particularly north of 35°N and south of 20°N.

3.2.4. South Africa 2013 event

The South Africa 2013 event, which occurred in austral autumn, contributed to winter rainfall in South Africa [7]. With an IWV range of ~7 to 47 kg m- ^{2}, this event reflects considerable moisture transport in a strong AR. The scatter plot in Figure 11 (a) shows a strong positive correlation between RO and ERA5 IWV values with a RMSE of 4.08 kg m^{-2}, a Mean Bias of - 2.22 kg m^{-2} and a slope of 0.83. The metrics are similar to the 2009 event (slope: 0.82, RMSE: 4.37 kg m^{-2}). However, discrepancies are more apparent at higher IWV values, particularly above 40 kg m^{-2}. This event additionally shows good data coverage of the AR event (see Figure 11(b)) itself and a total of 95 datapoints available for comparison.

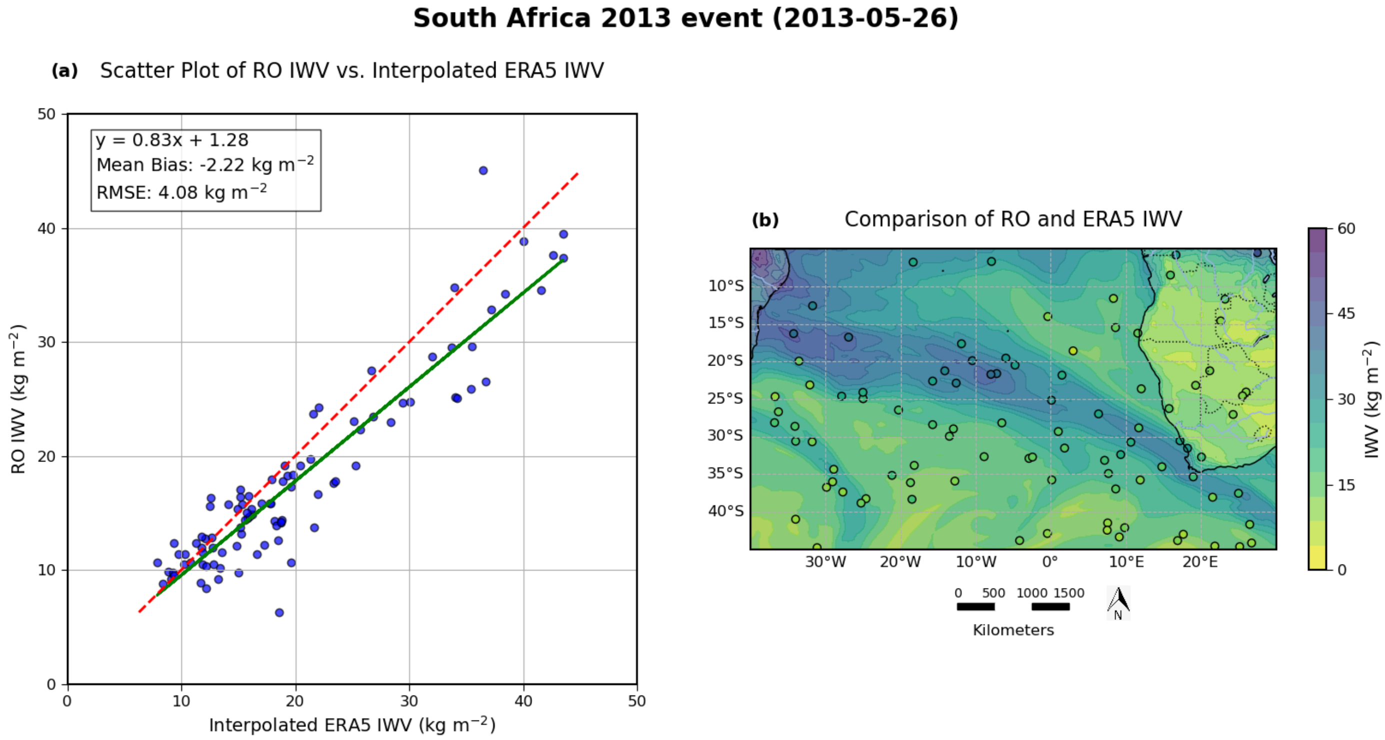

Figure 11. Analysis of the South Africa 2013 event. **(a)** Scatter Plot of RO versus ERA5 IWV. **(b)** IWV from ERA5 (map) and from RO (filled circles).

The spatial distribution map in Figure 11 (b) highlights ERA5 capturing broad IWV patterns across the South Atlantic and coastal Southern Africa, showing high values over the ocean (30-45 kg m^{-2}) and lower values inland (15-30 kg m^{-2}). ERA5 aligns well with RO data over land, particularly in Namibia and Angola, but shows higher IWV values over the Atlantic between 20°S and 30°S, with ERA5 reporting up to 45 kg m^{-2} while RO data provide comparatively drier values.

3.2.5. MENA 2017 event

Driven by moisture originating over the Red and Mediterranean Seas, this event triggered flooding and snowmelt across the Middle East and Northern Africa. Concurring with increased Saharan dust transport, this AR demonstrates the complex impacts of such events [15, 57]. The RMSE value of 4.29 kg m^{-2}, indicates relatively good agreement overall, though notable outliers are present (Figure 12 (a)). Additionally, the moderate Mean Bias of -1.66 kg m^{-2} and the steepest slope (0.88) among all investigated cases, reflect the strongest linear relationship between ERA5 and RO IWV datasets.

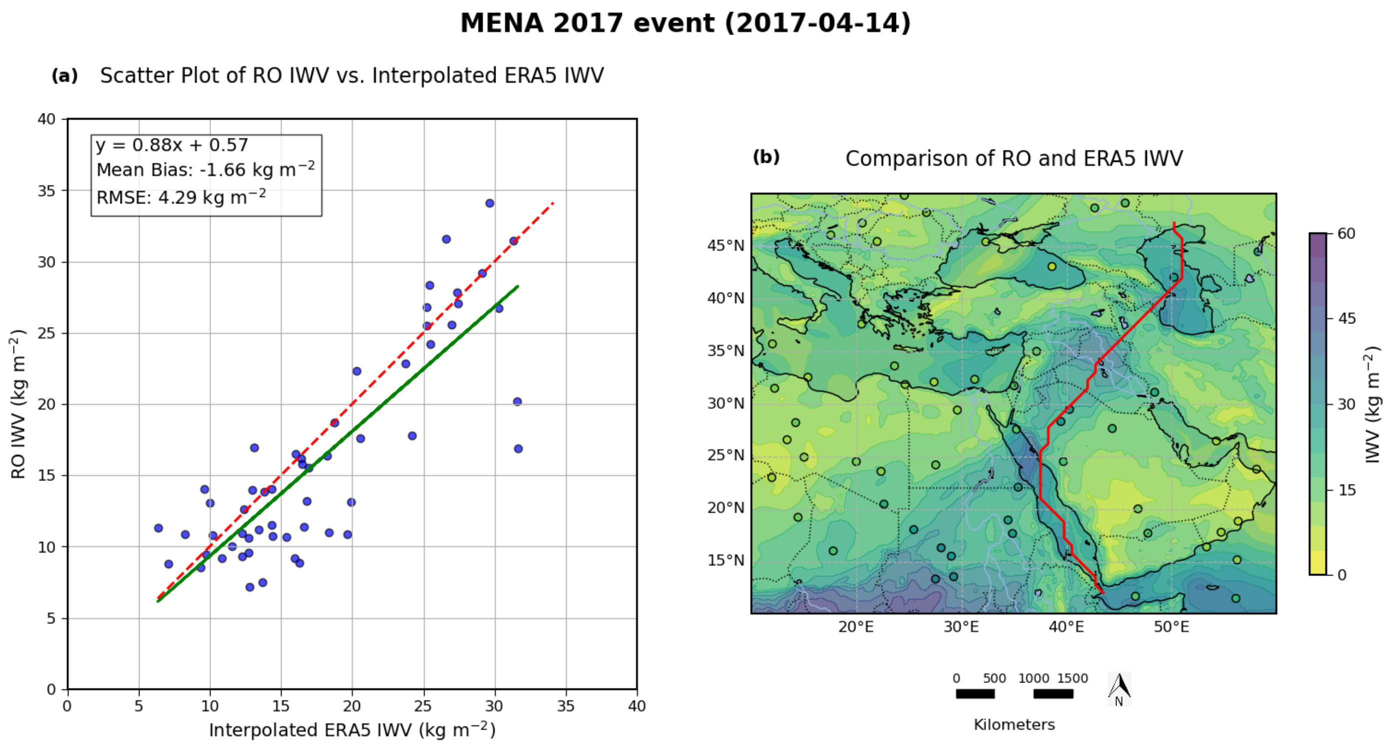

Figure 12. Analysis of the MENA 2017 event. **(a)** Scatter Plot of RO versus ERA5 IWV. **(b)** IWV from ERA5 (map) and from RO (filled circles) including the path of the AR (red).

The spatial distribution map (Figure 12 (b)) reveals good agreement between ERA5 and RO over North Africa, where IWV is lower (10–20 kg m^{-2}). The red line displays the AR path. It was plotted based on the AR axis coordinates. Over the Persian Gulf and parts of Saudi Arabia, ERA5 captures the broad moisture pattern (15–30 kg m^{-2}) but tends to report moisture values in areas with rapid moisture transport, particularly in the Middle East. The higher values of IWV in regions with fast changing conditions arise from model limitations resolving small-scale transport dynamics and the parameterization of convection and vertical mixing processes.

3.2.6. Mauritania 2019 event

The Mauritania 2019 event showcased how dynamic and thermodynamic processes, including a midlatitude system, subtropical jet, and orography, drove extreme rainfall in March [61]. The resulting floods in Iran caused severe damage.

Figure 13 (a) displays the highest RMSE (4.53 kg m^{-2}), indicating the weakest agreement between the two datasets and the greatest variability. The IWV in the scatter plot ranges from 4 to 47 kg m^{-2}. The Mean Bias of - 1.82 kg m^{-2} highlights ERA5′s tendency to report elevated IWV values, particularly at lower moisture levels, as reflected in the large intercept of 3.26 kg m^{-2} (highest amongst all events). The weakest linear relationship is evident by the smallest slope (0.72) among the events. Discrepancies are most pronounced at lower IWV values, contrasting with other events where higher IWV values showed greater deviations.

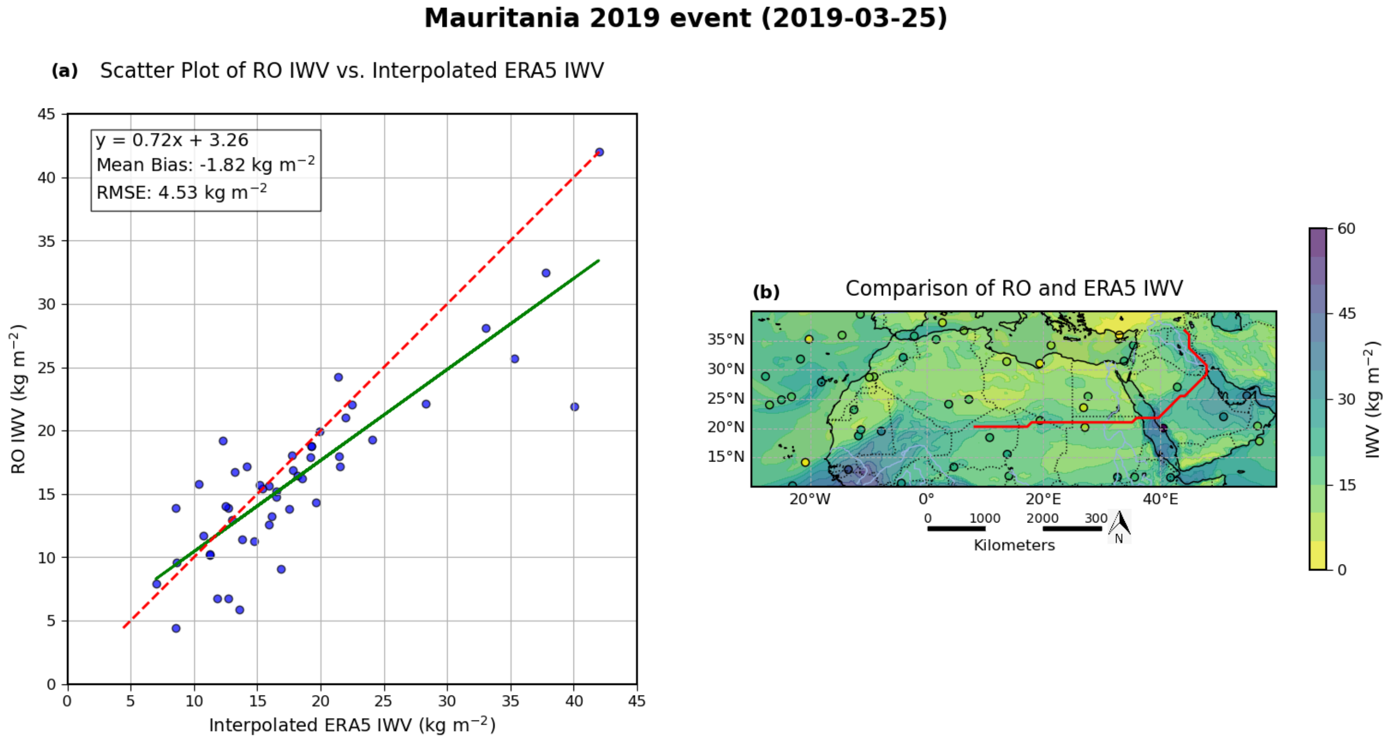

Figure 13. Analysis of the Mauritania 2019 event. **(a)** Scatter Plot of RO versus ERA5 IWV. **(b)** IWV from ERA5 (map) and from RO (filled circles) including the path of the AR (red).

Despite these discrepancies, Figure 13 (b) shows that ERA5 captures the large-scale moisture transport across North Africa and the Middle East. However, ERA5 exhibits a positive bias in regions of high IWV, such as Northwest Africa and Saudi Arabia. Limited satellite humidity observations over land likely contribute to these biases and the less distinct depiction of the AR path in ERA5. For clarity, the AR path is highlighted in red to indicate the observed trajectory.

Overall, good agreement between ERA5 and RO is prevailing for all events. The slopes between 0.72 and 0.88 and consistent negative biases show systematic differences between the two datasets. This finding is consistent with a previous study [21], that showed that GNSS-RO (CDAAC and WEGC) aligns closely with SSMI/S data, both consistently reporting lower IWV values than ERA5. This agreement underscores that the observed differences are due to a combination of ERA5's and the RO′s representation of moisture, rather than a singular overestimation or underestimation by one dataset. RMSE values, ranging from 3.11 kg m^{-2} to 4.53 kg m^{-2}, are moderate, indicating that ERA5 generally performs well when compared to RO but could benefit from further refinement.

Among the events, the South Africa 2009 event stands out with the largest number of RO events that provide a robust evaluation, while the Mauritania 2019 event is impacted by a decrease in RO observations during that time. The primary reason is the limited availability of RO satellite observations on that specific date. This event exhibits the weakest performance by ERA5 with the highest RMSE, the lowest slope, and the largest intercept. The MENA 2017 event demonstrates a strong linear relationship (highest slope) and minimal baseline offset (lowest intercept), suggesting ERA5 captures IWV variations well. The MENA 2010 event stands out with the strongest agreement between RO and ERA5 IWV, with the lowest RMSE and mean bias, reflecting accurate ERA5 representation.

The analysis reveals that ERA5 generally performs well in capturing IWV during moderate AR events (e.g., MENA 2010 and MENA 2017), where IWV ranges are narrower, and biases are smaller. However, for stronger ARs with higher IWV values (e.g., Morocco

2010 and South Africa 2013), ERA5 struggles to accurately represent extreme moisture levels, leading to higher RMSE and larger systematic biases. The weakest agreement, seen in the Mauritania 2019 event, emphasizes the need for further refinement of ERA5 to better capture IWV variability during high-intensity ARs.

4. Conclusion

The findings of this research highlight the characteristics, seasonal trends, and regional differences in AR activity across Africa from 2009 to 2019. Additionally, this study evaluates the effectiveness of ERA5 compared to GNSS RO datasets in representing IWV during landfalling falling AR events. Key findings are summarized below:

1. **Annual Frequency and Distribution**
   A total of 1,730 AR events made landfall in Africa during the study period, with a yearly average of 159 ARs. The years 2011 and 2018 showed the highest AR counts with 174 and 171 events respectively, correlating with La Niña years. El Niño years (2009 and 2015/16) did not show a significant impact, as the AR count was lowest for the whole study period in 2009 with 139 events making landfall but comparably high for 2016 (166 ARs).
2. **Seasonal Distribution and Monthly Trend**
   Peaks of average monthly ARs counts for the whole continent occurred in January (188 ARs), February (181 ARs), March (189 ARs) and October (163 ARs). The most active season, with 47 ARs on average, was austral summer (DJF), peaking in 2019 (59 ARs). Consistently the least activity, with the lowest count in 2013 (18ARs) was austral winter (JJA). SON (austral spring) showed moderate activity from 29 ARs in 2009 and 2014 up to 52 ARs in 2010. The second most active season, MAM (austral autumn), showed peak activity in 2014 (56 ARs) and a low in 2015 and 2019 (37 ARs).
3. **Regional Differences: Southern vs. Northern Africa**
   Southern Africa experienced consistently higher AR activity throughout the year, peaking in austral summer (DJF). Northern Africa, however, saw a distinct seasonality, with AR events peaking in boreal winter (DJF) and spring (MAM), reflecting the region's interactions with mid-latitude weather systems and seasonal shifts in the ITCZ.
4. **Interannual Variability**
   The frequency of AR events varied from year to year, with peaks in 2011 and 2018 and lower counts in 2009 and 2013, indicating the influence of large-scale atmospheric dynamics.
5. **Event-Specific Insights**
   The MENA 2010 event showed the strongest agreement between ERA5 and GNSS RO IWV values, with the lowest RMSE (3.11 kg m^{-2}). While the Mauritania 2019 event demonstrated the weakest ERA5 performance, with the highest RMSE (4.53 kg m^{-2}) and the largest intercept, indicating challenges in capturing extreme moisture conditions.
6. **IWV and Pattern Consistency**
   The analyzed AR events demonstrate a good overall agreement between ERA5 and GNSS RO IWV data. Acknowledging the fact that RO misses a part of the water vapor in the lowermost part of the profiles, but also that ERA5 reanalyses tend to be to wet [21], we conclude-that this systematic difference is due to both ERA5 and RO. Despite this, ERA5 effectively captured large-scale IWV patterns and high-moisture zones associated with AR events.

Comparisons between ERA5 and RO are currently somewhat limited due to a comparatively small number of RO profiles. However, expected increases in RO numbers in the future will allow for more detailed comparisons and for studies of AR events in other parts of the world.

Author Contributions: Conceptualization: LM, BR and UF; methodology: LM and BR; software: LM and BR; validation: LM, BR and UF; formal analysis: LM and BR; investigation: LM; resources: LM and BR; data curation: LM; writing—original draft preparation: LM; writing—review and editing: LM, BF and UF; visualization: LM; supervision: BR and UF; project administration: LM All authors have read and agreed to the published version of the manuscript.

Funding: This work was funded by the Austrian Science Fund (FWF) under Research Grant W1256 (Doctoral Programme on 'Climate Change: Uncertainties, Thresholds and Coping Strategies), and by the University of Graz.

Data Availability Statement:

- **ERA5 reanalysis data set:**
  Copernicus Climate Change Service, Climate Data Store, (2023): ERA5 hourly data on single levels from 1940 to present. Copernicus Climate Change Service (C3S) Climate Data Store (CDS), DOI: 10.24381/cds.adbb2d47
- **IPART:** https://github.com/ihesp/IPART
- **ARtracks:** https://github.com/dominiktraxl/artracks
- **RO data:** Index of /gnss-ro/

The original contributions presented in the study are included in the article, further inquiries can be directed to the corresponding author.

Conflicts of Interest: The authors declare no conflicts of interest.

References

1. Zhu, Y.; Newell, R.E. Atmospheric Rivers and Bombs. *Geophys Res Lett* 1994, *21*, 1999–2002, doi: 10.1029/94GL01710.
2. Dacre, H.F.; Clark, P.A.; Martinez-Alvarado, O.; Stringer, M.A.; Lavers, D.A. How Do Atmospheric Rivers Form? *Bull Am Meteorol Soc* 2015, *96*, 1243–1255, doi:10.1175/BAMS-D-14-00031.1.
3. Gimeno, L.; Nieto, R.; Vázquez, M.; Lavers, D. Atmospheric Rivers: A Mini-Review. *Front Earth Sci (Lausanne)* 2014, *2*, doi:10.3389/feart.2014.00002.
4. Akbary, M.; Salimi, S.; Hosseini, S.A.; Hosseini, M. Spatio-Temporal Changes of Atmospheric Rivers in the Middle East and North Africa Region. *International Journal of Climatology* 2019, *39*, 3976–3986, doi: 10.1002/joc.6052.
5. Esfandiari, N.; Shakiba, A. The Extraordinary Atmospheric Rivers Analysis over the Middle East: Large-Scale Drivers, Structure, Effective Sources, and Precipitation Characterization. *Dynamics of Atmospheres and Oceans* 2024, *105*, 101430, doi:10.1016/j.dynatmoce.2023.101430.
6. Salimi, S.; Helali, J.; Lotfi, M.; Momenzadeh, H.; Hosseini, S.A.; Asaadi Oskuei, E.; Izadi, A.; Yarmoradi, Z.; Bakhshi, I. Investigating the Origin and Pathways of Atmospheric Rivers in the World. *Theor Appl Climatol* 2020, *142*, 165–175, doi:10.1007/s00704-020-03299-w.
7. Blamey, R.C.; Ramos, A.M.; Trigo, R.M.; Tomé, R.; Reason, C.J.C. The Influence of Atmospheric Rivers over the South Atlantic on Winter Rainfall in South Africa. *J Hydrometeorol* 2018, *19*, 127–142, doi:10.1175/JHM-D-17-0111.1.
8. Ramos, A.M.; Blamey, R.C.; Algarra, I.; Nieto, R.; Gimeno, L.; Tomé, R.; Reason, C.J.C.; Trigo, R.M. From Amazonia to Southern Africa: Atmospheric Moisture Transport through Low-Level Jets and Atmospheric Rivers. *Ann N Y Acad Sci* 2019, *1436*, 217–230, doi:10.1111/nyas.13960.
9. Ramos, A.M.; Trigo, R.M.; Tomé, R.; Liberato, M.L.R. Impacts of Atmospheric Rivers in Extreme Precipitation on the European Macaronesian Islands. *Atmosphere (Basel)* 2018, *9*, doi:10.3390/atmos9080325.
10. Gimeno-Sotelo, L.; Gimeno, L. Concurrent Extreme Events of Atmospheric Moisture Transport and Continental Precipitation: The Role of Landfalling Atmospheric Rivers. *Atmos Res* 2022, *278*, 106356, doi:10.1016/j.atmosres.2022.106356.
11. Reason, C.J.C. Subtropical Indian Ocean SST Dipole Events and Southern African Rainfall. *Geophys Res Lett* 2001, *28*, 2225–2227, doi:10.1029/2000GL012735.
12. Thandlam, V.; Rutgersson, A.; Sahlée, E. Rivers in the Sky: An Introduction and Review on Recent Studies 2022.
13. Conway, D. Adapting Climate Research for Development in Africa. *WIREs Climate Change* 2011, *2*, 428–450, doi:10.1002/wcc.115.
14. Vaughan, C.; Hansen, J.; Roudier, P.; Watkiss, P.; Carr, E. Evaluating Agricultural Weather and Climate Services in Africa: Evidence, Methods, and a Learning Agenda. *WIREs Climate Change* 2019, *10*, e586, doi:10.1002/wcc.586.
15. Dezfuli, A.; Bosilovich, M.G.; Barahona, D. A Dusty Atmospheric River Brings Floods to the Middle East. *Geophys Res Lett* 2021, *48*, e2021GL095441, doi:10.1029/2021GL095441.
16. De Longueville, F.; Hountondji, Y.-C.; Henry, S.; Ozer, P. What Do We Know about Effects of Desert Dust on Air Quality and Human Health in West Africa Compared to Other Regions? *Science of The Total Environment* 2010, *409*, 1–8, doi:10.1016/j.scitotenv.2010.09.025.
17. Khouakhi, A.; Driouech, F.; Slater, L.; Waine, T.; Chafki, O.; Chehbouni, A.; Raji, O. Atmospheric Rivers and Associated Extreme Rainfall over Morocco. *International Journal of Climatology* 2022, *42*, 7766–7778, doi:10.1002/joc.7676.

18. Knippertz, P.; Martin, J.E. Tropical Plumes and Extreme Precipitation in Subtropical and Tropical West Africa. *Quarterly Journal of the Royal Meteorological Society* 2005, *131*, 2337–2365, doi:10.1256/qj.04.148.
19. Gimeno, L.; Dominguez, F.; Nieto, R.; Trigo, R.; Drumond, A.; Reason, C.J.C.; Taschetto, A.S.; Ramos, A.M.; Kumar, R.; Marengo, J. Major Mechanisms of Atmospheric Moisture Transport and Their Role in Extreme Precipitation Events. *Annu Rev Environ Resour* 2016, *41*, 117–141, doi:10.1146/annurev-environ-110615-085558.
20. Wainwright, C.M.; Finney, D.L.; Kilavi, M.; Black, E.; Marsham, J.H. Extreme Rainfall in East Africa, October 2019–January 2020 and Context under Future Climate Change. *Weather* 2021, *76*, 26–31, doi:10.1002/wea.3824.
21. Rahimi, B.; Foelsche, U. Observing Atmospheric Rivers Using GNSS Radio Occultation Data. *Atmospheric Measurement Techniques Discussions* 2024, *2024*, 1–40, doi:10.5194/amt-2024-81.
22. Innerkofler, J.; Kirchengast, G.; Schwärz, M.; Marquardt, C.; Andres, Y. GNSS Radio Occultation Excess-Phase Processing for Climate Applications Including Uncertainty Estimation. *Atmos Meas Tech* 2023, *16*, 5217–5247, doi:10.5194/amt-16-5217-2023.
23. Hersbach, H.; Bell, B.; Berrisford, P.; Hirahara, S.; Horányi, A.; Muñoz-Sabater, J.; Nicolas, J.; Peubey, C.; Radu, R.; Schepers, D.; et al. The ERA5 Global Reanalysis. *Quarterly Journal of the Royal Meteorological Society* 2020, *146*, 1999–2049, doi:10.1002/qj.3803.
24. Copernicus Knowledge Base: ERA5 Data Documentation.
25. University Corporation for Atmospheric Research CDAAC: COSMIC Data Analysis and Archive Center.
26. Steiner, A.K.; Lackner, B.C.; Ladstädter, F.; Scherllin-Pirscher, B.; Foelsche, U.; Kirchengast, G. GPS Radio Occultation for Climate Monitoring and Change Detection. *Radio Sci* 2011, *46*, doi:10.1029/2010RS004614.
27. Steiner, A.K.; Kirchengast, G.; Foelsche, U.; Kornblueh, L.; Manzini, E.; Bengtsson, L. GNSS Occultation Sounding for Climate Monitoring. *Physics and Chemistry of the Earth, Part A: Solid Earth and Geodesy* 2001, *26*, 113–124, doi:10.1016/S1464-1895(01)00034-5.
28. Foelsche, U.; Borsche, M.; Steiner, A.K.; Gobiet, A.; Pirscher, B.; Kirchengast, G.; Wickert, J.; Schmidt, T. Observing Upper Troposphere–Lower Stratosphere Climate with Radio Occultation Data from the CHAMP Satellite. *Clim Dyn* 2008, *31*, 49–65, doi:10.1007/s00382-007-0337-7.
29. Bevis, M.; Businger, S.; Herring, T.A.; Rocken, C.; Anthes, R.A.; Ware, R.H. GPS Meteorology: Remote Sensing of Atmospheric Water Vapor Using the Global Positioning System. *Journal of Geophysical Research: Atmospheres* 1992, *97*, 15787–15801, doi:10.1029/92JD01517.
30. Kursinski, E.R.; Hajj, G.A.; Hardy, K.R.; Romans, L.J.; Schofield, J.T. Observing Tropospheric Water Vapor by Radio Occultation Using the Global Positioning System. *Geophys Res Lett* 1995, *22*, 2365–2368, doi:10.1029/95GL02127.
31. Bouma, H.R.; Stoew, B. GPS Observations of Daily Variations in the Atmospheric Water Vapor Content. *Physics and Chemistry of the Earth, Part A: Solid Earth and Geodesy* 2001, *26*, 389–392, doi:10.1016/S1464-1895(01)00071-0.
32. Gilpin, S.; Rieckh, T.; Anthes, R. Reducing Representativeness and Sampling Errors in Radio Occultation–Radiosonde Comparisons. *Atmos Meas Tech* 2018, *11*, 2567–2582, doi:10.5194/amt-11-2567-2018.
33. Rieckh, T.; Anthes, R.; Randel, W.; Ho, S.-P.; Foelsche, U. Tropospheric Dry Layers in the Tropical Western Pacific: Comparisons of GPS Radio Occultation with Multiple Data Sets. *Atmos Meas Tech* 2017, *10*, 1093–1110, doi:10.5194/amt-10-1093-2017.
34. Neiman, P.J.; Ralph, F.M.; Wick, G.A.; Kuo, Y.-H.; Wee, T.-K.; Ma, Z.; Taylor, G.H.; Dettinger, M.D. Diagnosis of an Intense Atmospheric River Impacting the Pacific Northwest: Storm Summary and Offshore Vertical Structure Observed with COSMIC Satellite Retrievals. *Mon Weather Rev* 2008, *136*, 4398–4420, doi:10.1175/2008MWR2550.1.

35. Murphy, M.J.; Haase, J.S. Evaluation of GNSS Radio Occultation Profiles in the Vicinity of Atmospheric Rivers. *Atmosphere (Basel)* 2022, *13*, doi:10.3390/atmos13091495.
36. Ma, Z.; Kuo, Y.-H.; Ralph, F.M.; Neiman, P.J.; Wick, G.A.; Sukovich, E.; Wang, B. Assimilation of GPS Radio Occultation Data for an Intense Atmospheric River with the NCEP Regional GSI System. *Mon Weather Rev* 2011, *139*, 2170–2183, doi:10.1175/2011MWR3342.1.
37. Xu, G.; Ma, X.; Chang, P.; Wang, L. Image-Processing-Based Atmospheric River Tracking Method Version 1 (IPART-1). *Geosci Model Dev* 2020, *13*, 4639–4662, doi:10.5194/gmd-13-4639-2020.
38. Traxl, D. ARtracks - a Global Atmospheric River Catalogue Based on ERA5 and IPART (1.0.0) [Data Set]. Zenodo. 2022.
39. Reid, K.J.; King, A.D.; Lane, T.P.; Short, E. The Sensitivity of Atmospheric River Identification to Integrated Water Vapor Transport Threshold, Resolution, and Regridding Method. *Journal of Geophysical Research: Atmospheres* 2020, *125*, e2020JD032897, doi:10.1029/2020JD032897.
40. Ikechukwu, M.N.; Ebinne, E.; Idorenyin, U.; Raphael, N.I. Accuracy Assessment and Comparative Analysis of IDW, Spline and Kriging in Spatial Interpolation of Landform (Topography): An Experimental Study. *Scientific Research* 2017.
41. Karydas, C.; Gitas, I.; Koutsogiannaki, E.; Lydakis Simantiris, N.; Silleos, G. Evaluation of Spatial Interpolation Techniques for Mapping Agricultural Topsoil Properties in Crete. *EARSel* 2009, *8*.
42. Das, M.; Hazra, A.; Sarkar Ray, A.; Bhattacharya, S.; Banik, P. Comparison of Spatial Interpolation Methods for Estimation of Weekly Rainfall in West Bengal, India. *Mausam* 2017, *68*, 41–50, doi:10.54302/mausam.v68i1.407.
43. Ali, G.; Sajjad, M.; Kanwal, S.; Xiao, T.; Khalid, S.; Shoaib, F.; Gul, H.N. Spatial–Temporal Characterization of Rainfall in Pakistan during the Past Half-Century (1961–2020). *Sci Rep* 2021, *11*, 6935, doi:10.1038/s41598-021-86412-x.
44. Choi, D.-S.; Lee, Y.-J.; Ko, M.-J. Utilization and Verification of Inverse Distance Weighting (IDW) Interpolation Technology for Predicting Solar Radiation of Photovoltaic System. *KIEAE Journal* 2022, *22*, 5–12, doi:10.12813/kieae.2022.22.1.005.
45. McClenny, E.E.; Ullrich, P.A.; Grotjahn, R. Sensitivity of Atmospheric River Vapor Transport and Precipitation to Uniform Sea Surface Temperature Increases. *Journal of Geophysical Research: Atmospheres* 2020, *125*, e2020JD033421, doi:10.1029/2020JD033421.
46. Norris, J.R.; Ralph, F.M.; Demirdjian, R.; Cannon, F.; Blomquist, B.; Fairall, C.W.; Spackman, J.R.; Tanelli, S.; Waliser, D.E. The Observed Water Vapor Budget in an Atmospheric River over the Northeast Pacific. *J Hydrometeorol* 2020, *21*, 2655–2673, doi:10.1175/JHM-D-20-0048.1.
47. LAMPINEN, M.; ASSAD, M.E.L.H.A.J.; Curd, E.F. 4 - PHYSICAL FUNDAMENTALS. In *Industrial Ventilation Design Guidebook*; Goodfellow, H., Tähti, E., Eds.; Academic Press: San Diego, 2001; pp. 41–171 ISBN 978-0-12-289676-7.
48. Trnka, M.; Žalud, Z.; Eitzinger, J.; Dubrovský, M. Global Solar Radiation in Central European Lowlands Estimated by Various Empirical Formulae. *Agric For Meteorol* 2005, *131*, 54–76, doi: 10.1016/j.agrformet.2005.05.002.
49. Yang, F.; White, M.A.; Michaelis, A.R.; Ichii, K.; Hashimoto, H.; Votava, P.; Zhu, A.-X.; Nemani, R.R. Prediction of Continental-Scale Evapotranspiration by Combining MODIS and AmeriFlux Data Through Support Vector Machine. *IEEE Transactions on Geoscience and Remote Sensing* 2006, *44*, 3452–3461, doi:10.1109/TGRS.2006.876297.

50. Hu, X.; Weng, Q. Estimating Impervious Surfaces from Medium Spatial Resolution Imagery Using the Self-Organizing Map and Multi-Layer Perceptron Neural Networks. *Remote Sens Environ* 2009, *113*, 2089–2102, doi:10.1016/j.rse.2009.05.014.
51. Bozkurt, D.; Sen, O.L.; Ezber, Y.; Guan, B.; Viale, M.; Caglar, F. Influence of African Atmospheric Rivers on Precipitation and Snowmelt in the Near East's Highlands. *Journal of Geophysical Research: Atmospheres* 2021, *126*, e2020JD033646, doi:10.1029/2020JD033646.
52. Massoud, E.; Massoud, T.; Guan, B.; Sengupta, A.; Espinoza, V.; De Luna, M.; Raymond, C.; Waliser, D. Atmospheric Rivers and Precipitation in the Middle East and North Africa (MENA). *Water (Basel)* 2020, *12*, doi:10.3390/w12102863.
53. Adusumilli, S.; Borsa, A.A.; Fish, M.A.; McMillan, H.K.; Silverii, F. A Decade of Water Storage Changes Across the Contiguous United States From GPS and Satellite Gravity. *Geophys Res Lett* 2019, *46*, 13006–13015, doi:10.1029/2019GL085370.
54. NOAA Equatorial Pacific Sea Surface Temperatures (SST).
55. NOAA What Are El Niño and La Niña? 2024.
56. NOAA Monthly Climate Timeseries: Niño 3.4 SST.
57. Francis, D.; Fonseca, R.; Nelli, N.; Bozkurt, D.; Picard, G.; Guan, B. Atmospheric Rivers Drive Exceptional Saharan Dust Transport towards Europe. *Atmos Res* 2022, *266*, 105959, doi:10.1016/j.atmosres.2021.105959.
58. Nash, D.; Waliser, D.; Guan, B.; Ye, H.; Ralph, F.M. The Role of Atmospheric Rivers in Extratropical and Polar Hydroclimate. *Journal of Geophysical Research: Atmospheres* 2018, *123*, 6804–6821, doi:10.1029/2017JD028130.
59. Guan, B.; Waliser, D.E.; Ralph, F.M. Global Application of the Atmospheric River Scale. *Journal of Geophysical Research: Atmospheres* 2023, *128*, e2022JD037180, doi:10.1029/2022JD037180.
60. Guan, B.; Waliser, D.E. Atmospheric Rivers in 20 Year Weather and Climate Simulations: A Multimodel, Global Evaluation. *Journal of Geophysical Research: Atmospheres* 2017, *122*, 5556–5581, doi:10.1002/2016JD026174.
61. Dezfuli, A. Rare Atmospheric River Caused Record Floods across the Middle East. *Bull Am Meteorol Soc* 2020, *101*, E394–E400, doi:10.1175/BAMS-D-19-0247.1.